Electronic Supplementary Material (ESI) for Catalysis Science & Technology.

Supplementary Material

Transformation of Atomically Dispersed Platinum in SAPO-37 into Platinum Clusters: Catalyst for Ethylene Hydrogenation

Jorge E. Perez-Aguilar,[a] James T. Hughes,[b]* Cong-Yan Chen,[a,c] and Bruce C. Gates[a]*

[a]Department of Chemical Engineering, University of California, Davis, California 95616, United States
[b]Zeolyst International, Conshohocken, PA 19428, United States
[c]Chevron Technical Center, Richmond, CA 94802, United States

*Corresponding author. Email: bcgates@ucdavis.edu

Supporting Material

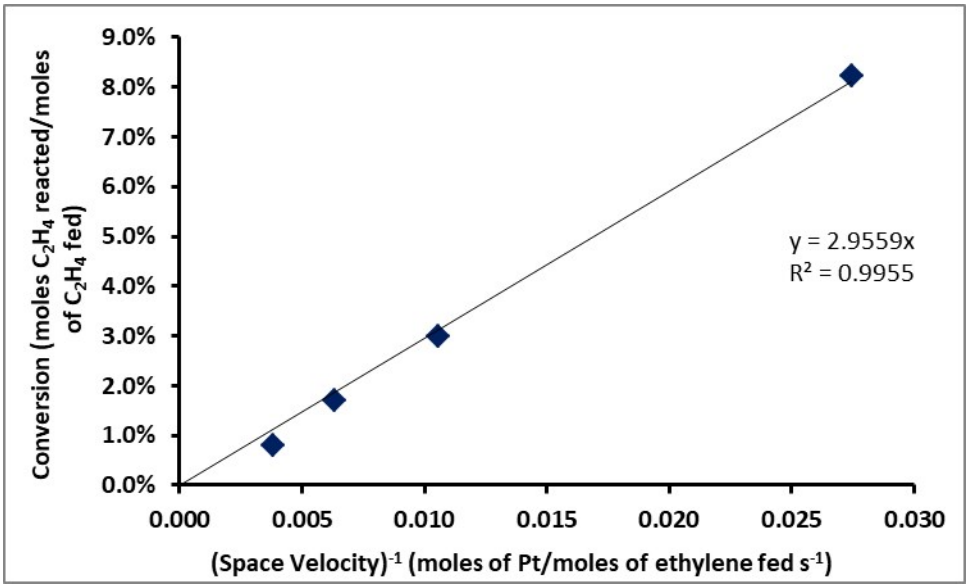

Fig. S1. Differential conversion of ethylene; the catalyst was initially present as platinum complexes supported on SAPO-37. Reaction conditions: H_2 + C_2H_4 at 10:1 molar ratio at 303 K at atmospheric pressure. The linearity of this plot that passes through the origin demonstrates that the data determine rates (TOF values) directly as the slope of the line.

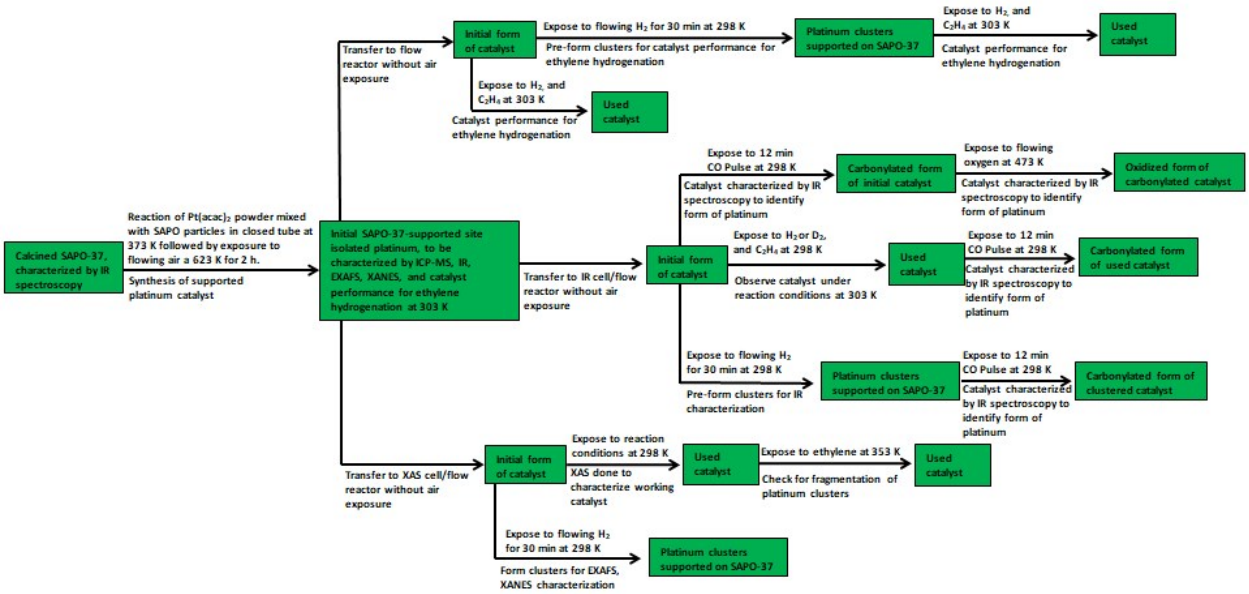

Scheme 1. Summary of treatment steps and methods of characterization of SAPO-37-supported platinum.

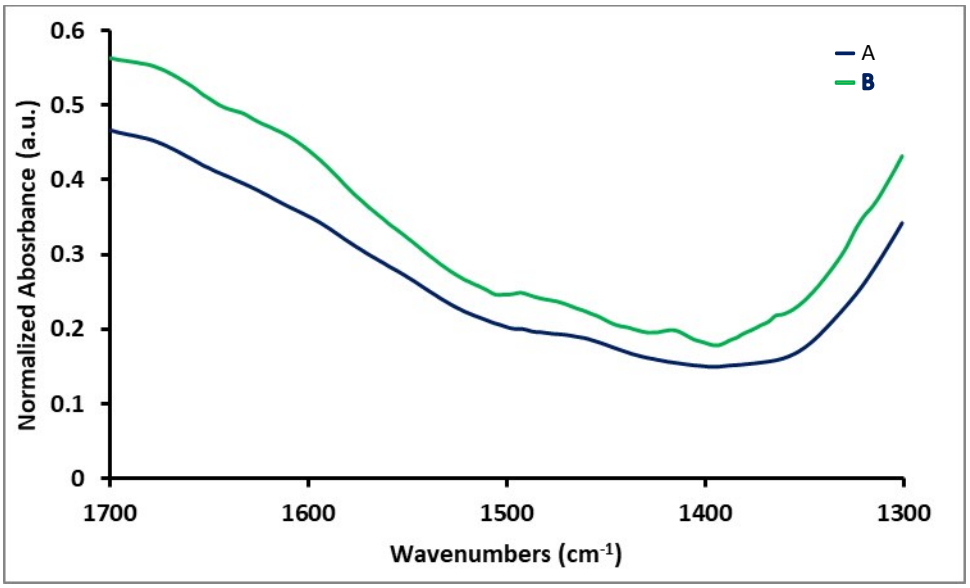

Fig. S2. IR spectra in the 1300–1700 cm^{-1} region characterizing the following samples: **A,** bare calcined SAPO-37; **B**, sample formed by reaction of SAPO-37 with $Pt(acac)_2$.

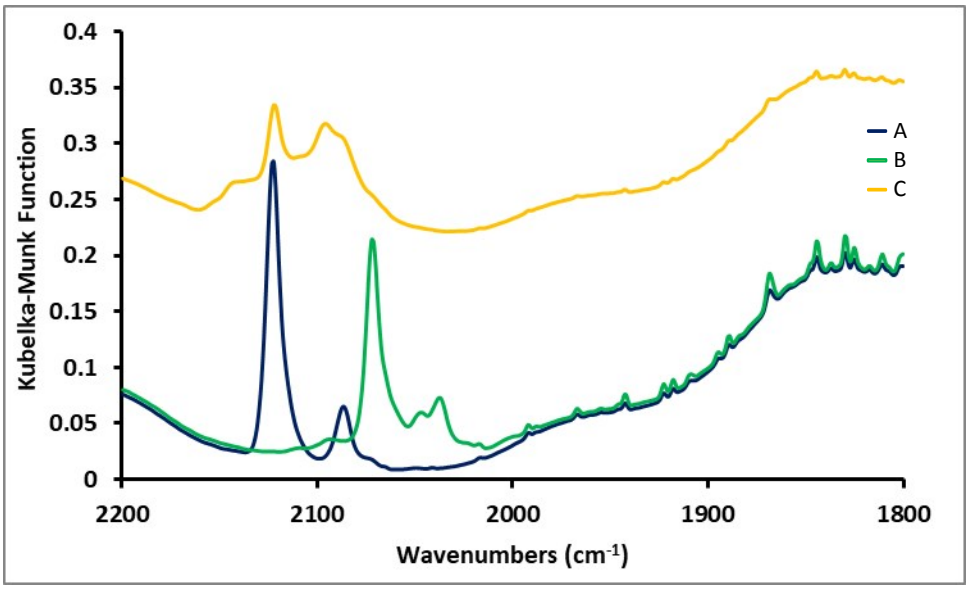

Fig. S3. DRIFTS spectra in the CO region of species formed by adsorption of isolated platinum on SAPO-37 after treatments. Spectrum **A** was recorded with the sample in contact with flowing helium (50 mL(NTP)/min), and Spectrum **B** is of the same sample in helium after it had been in contact with a 2 min pulse of ^{13}CO. Spectrum **C** is of the same sample under helium after a ^{12}CO pulse.

Bands at 2123 and 2090 cm^{-1} decreased in intensity while the bands at 2071 and 2039 cm^{-1} grew in as the ^{13}CO reacted with the sample (Fig. S3). The ratio of frequencies of ^{12}CO and ^{13}CO corresponds to the harmonic approximation.[1] Thus, bands at 2123 and 2088 cm^{-1} indicate the presence of CO on platinum species in different locations and/or oxidation states, with the inference based on reported results

characterizing platinum species on various zeolites,[2–4] and the shifts to 2071 and 2039 cm^{-1} confirm that ^{13}CO replaced ^{12}CO.[5] After a single ^{12}CO pulse to the same sample, the exchange to the initial CO bands was not reversed.

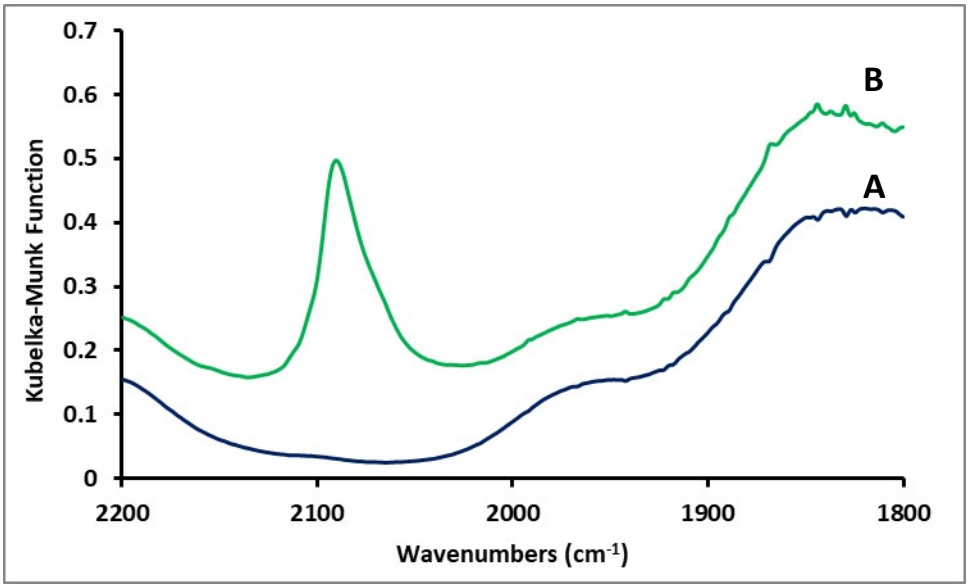

Fig. S4. DRIFTS spectra characterizing catalyst: **A**, SAPO-37 supported platinum complexes in flowing helium (50 mL(NTP)/min) at room temperature; **B**, same sample in helium(50 mL(NTP)/min) after a 12 minute CO (50 mL(NTP)/min) pulse and a 30 minute H_2 (50 mL(NTP)/min) treatment at room temperature.

Fig. S4 displays a single band as 2092 cm^{-1} that is expected for CO on platinum clusters.[2] EXAFS data given in Table S4 confirms the platinum clusters formed.

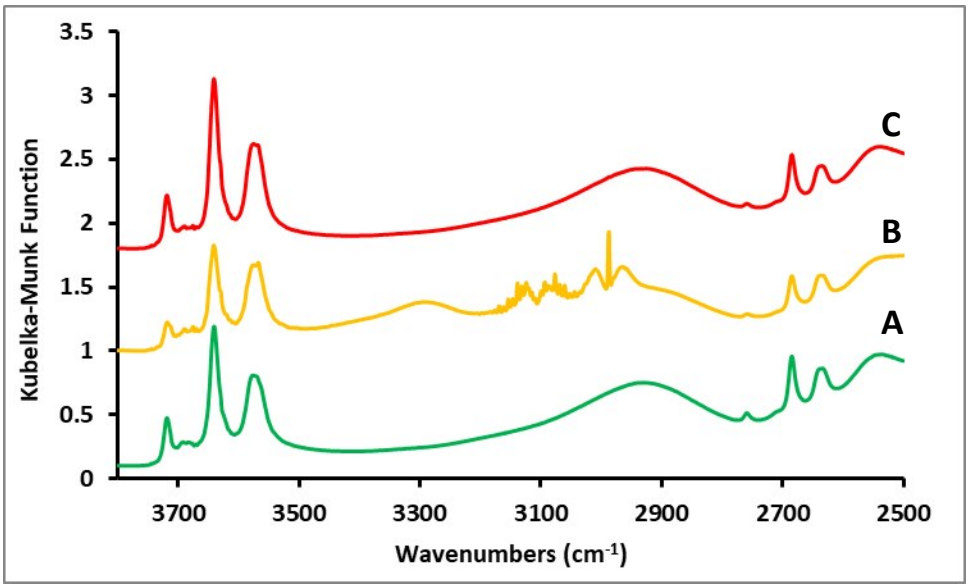

Fig. S5. DRIFTS spectra in the ν_{OH} and ν_{OD} regions characterizing (**A**) Platinum complexes on SAPO-37 in flowing D_2 and He (10 and 50 mL(NTP) min^{-1}) at 298 K and 1 bar, (**B**) the same sample in flowing C_2H_4

and He (10 and 50 mL(NTP) min^{-1}), (**C**) the same sample in flowing He (50 mL(NTP) min^{-1}). The broad peak in spectrum **B** (at 3300 cm^{-1}) is assigned to either the extra-framework silica (3718 cm^{-1}) or the Si–OH–Al Brønsted acid sites (3640 cm^{-1}) interacting with absorbed ethylene, consistent with data characterizing the silanols or Brønsted acid sites on HZSM-5 zeolite shifting to 3300 cm^{-1} when ethylene is absorbed.[6]

Fig. S5 displays the SAPO-37-supported platinum complexes after exposure to D_2 where the sample formed OD groups. This sample was then subsequently exposed to ethylene and a spectrum B shows that ethylene adsorbed on the OD and OH groups, when the reactor was purged with helium, the ethylene desorbed, as shown by the full recovery of the OH and OD band intensities.

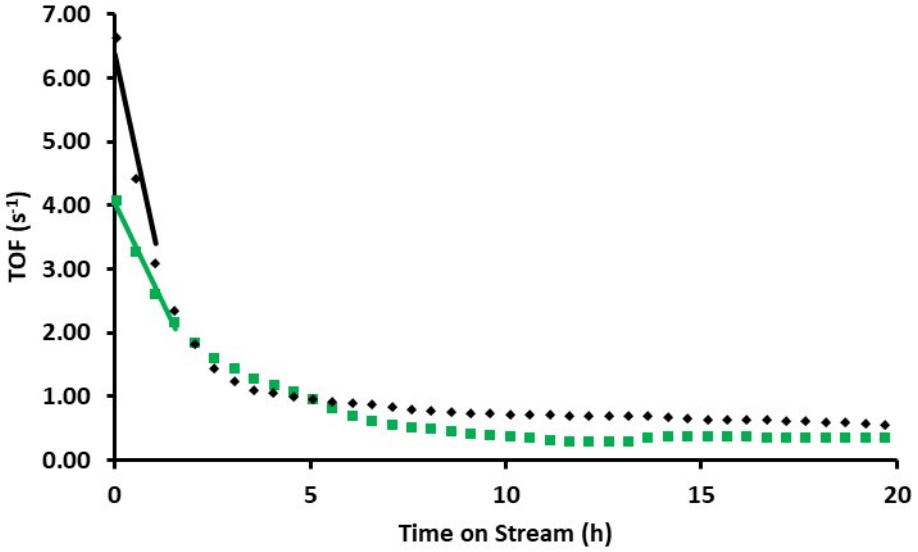

Fig. S6. Comparison of platinum supported SAPO-37 for ethylene conversion: performance of 1.4 ± 0.2 wt% platinum supported on SAPO-37 initially present as platinum clusters or atomically dispersed platinum for ethylene conversion catalysis in a once-through plug-flow reactor in the presence of H_2 at 303 K and 1 bar (molar H_2:C_2H_4 ratio = 4:1). The catalyst samples (in their initial forms) are identified by symbols shown in the figure: black ◆, SAPO-37-supported platinum clusters (molar H_2:C_2H_4 ratio = 1:10); green ■, atomically dispersed platinum supported on SAPO-37.

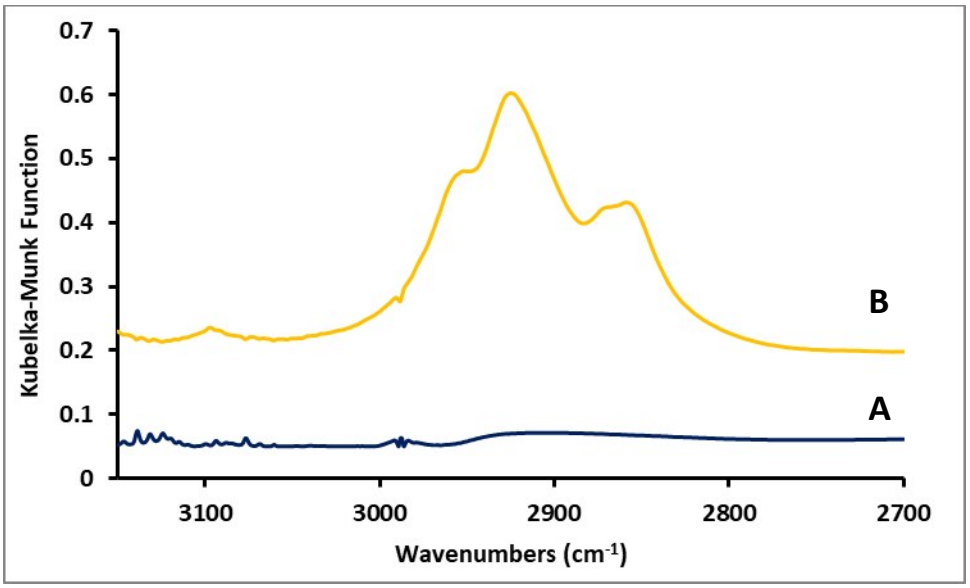

Fig. S7. DRIFTS spectra characterizing catalyst: **A**, SAPO-37 supported platinum complexes in flowing helium (50 mL(NTP)/min) at room temperature; **B**, same sample under reaction conditions (flow rates of 10 mL(NTP)/min of C_2H_4 and of H_2, and 90 mL(NTP)/min of helium) after 25 h in contact with flowing reactants at 303 K.

Fig. S7 shows intensities of peaks assigned to C−H vibrations (2970−2860 cm^{-1}), indicating carbonaceous deposits in the SAPO-37; similar results were observed for rhodium in zeolite and SAPO catalysts,[7] and they are regarded as the likely causes of the observed catalyst deactivation.

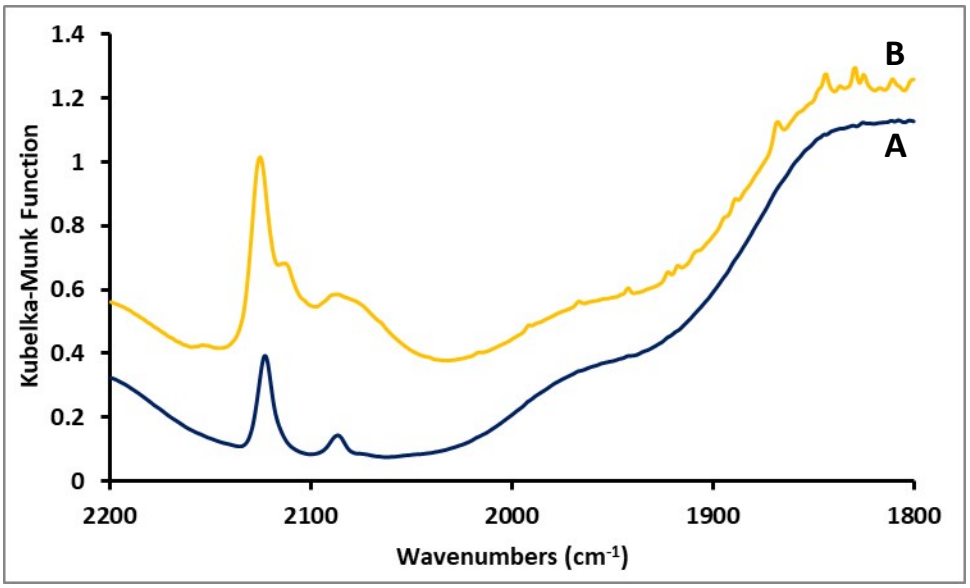

Fig. S8. DRIFTS spectra characterizing catalyst: **A**, SAPO-37 supported platinum complexes in flowing helium (50 mL(NTP)/min) at room temperature; **B**, same sample in flowing helium after a 12 min pulse of 10% CO in helium (50 mL(NTP)/min) and 24 h exposure of reactants at 303 K (4 and 40 mL(NTP)/min of C_2H_4 and H_2, and 56 mL(NTP)/min of helium.

Fig. S8 displays a change in the CO peaks after 24 h exposure to reaction conditions. There is an increase in intensity of the 2092 cm^{-1} peak that has been assigned to platinum clusters on SAPO-37.

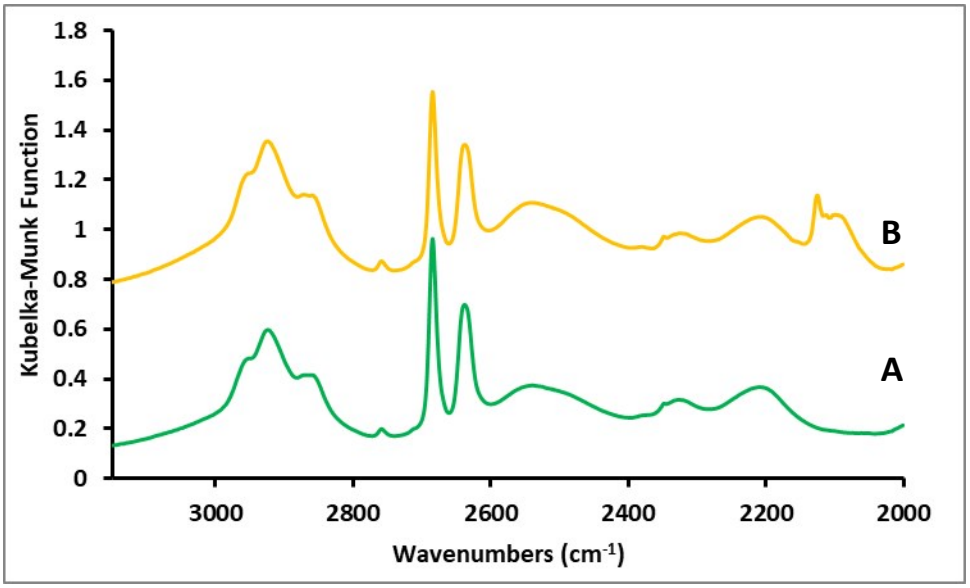

Fig. S9. DRIFTS spectra characterizing catalyst: **A**, SAPO-37 supported platinum complexes in flowing helium (50 mL(NTP)/min) at room temperature after a 24 h exposure of reactants at 303 K (2 and 20 mL(NTP)/min of C_2H_4 and D_2, and 78 mL(NTP)/min of helium; **B**, same sample in flowing helium after a 12 min pulse of 10% CO in helium (50 mL(NTP)/min). Bands at 2970−2860 cm^{-1} are assigned to C−H vibrations to carbonaceous deposits, as before.[7]

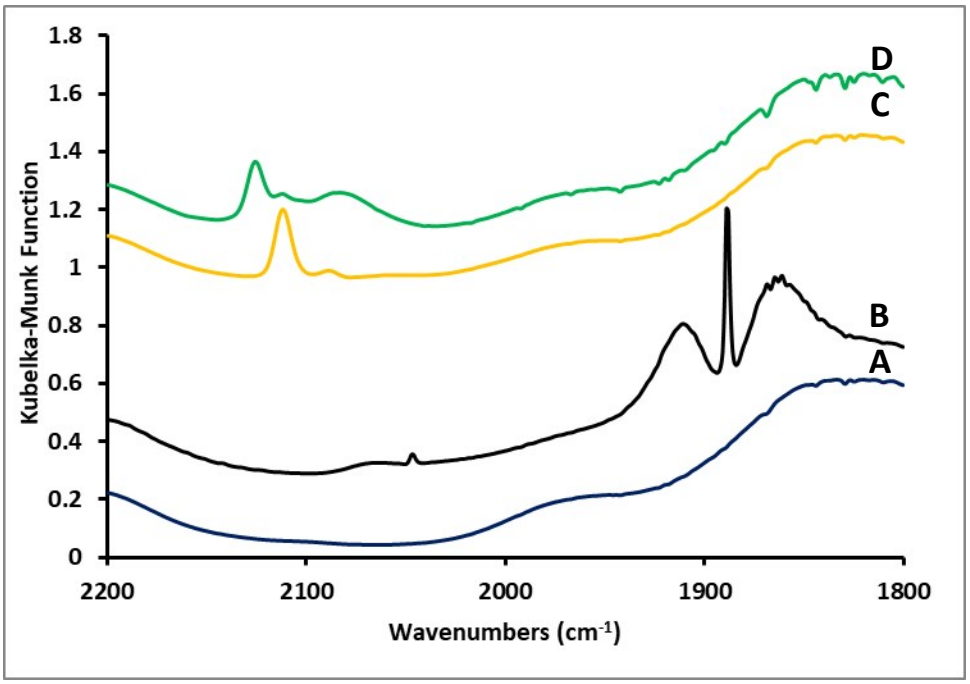

Fig. S10. DRIFTS spectra characterizing catalyst: **A**, SAPO-37 supported platinum complexes in flowing helium (50 mL(NTP)/min) at room temperature; **B** after a 24 h exposure of reactants at 303 K (40 and 4

mL(NTP)/min of C_2H_4 and H_2, and 56 mL(NTP)/min of helium; **C**, same sample in flowing helium; **D**, the same sample in flowing helium after a 12 min pulse of 10% CO in helium (50 mL(NTP)/min).

Table S1. Oxidation state estimation based on XAS white line intensities. Correspondence between white line intensity and oxidation state made based on reference compounds of known oxidation state. This relationship was used to estimate oxidation states for Pt/SAPO-37 following exposure to ethylene and reaction conditions.

Reference compound	**Normalized white line height, arbitrary units**	**Formal Pt oxidation state**
PtO_2	2.27	4
$Pt(acac)_2$	1.67	2
Pt foil	1.20	0
	Normalized white line height	**Estimated Pt oxidation state**
Pt/SAPO-37, 1.4 ± 0.2 wt%	1.74	2.2
Pt/SAPO-37, 1.4 ± 0.2 wt% platinum, after exposure to H_2 for 30 min	1.35	0.6

Ligands that might have been formed on the supported atomically dispersed platinum in the oxidation step of the synthesis could be thought to be acac ligands, but that this possibility is ruled out, as follows: The IR spectra (Fig. S2) indicate the complete removal of the acac ligands present in the precursor $Pt(acac)_2$ during the synthesis (including oxidation) at 623 K. Similar results were observed by Guzman *et al.*,[8] who found that temperatures above 573 K were needed for total removal of the acac ligands on from alumina-supported atomically dispersed gold made from $Au(CH_3)_2(acac)$.[8]

The ligands might also be thought to be peroxo ligands, but the XANES data weigh against this possibility, showing that the average platinum oxidation state was only slightly greater than +2 and not +4, which is common for platinum-group metal peroxo species.[9,10]

One might also suggest that CO ligands formed from the acac ligands during oxidation were present on the Pt, but the IR data rule out this possibility: in Spectrum A of Fig. S4, it is evident that there are no bands characterizing platinum carbonyls.

One might also suggest that OH ligands from the support migrated onto the Pt, but one would expect them to be more strongly bonded to the Al sites on the SAPO than to the platinum because of the negative formal charge of the alumina tetrahedra.

In summary, on the basis of our IR, XANES, and EXAFS data, we postulate that each platinum atom, on average, was bonded to two oxygen ligands of the SAPO support and to two other light scatterers, which could have been oxygen, but the data are not sufficient to identify these ligands.

Table S2. Examples of CO bonded to platinum species including IR band locations in the ν_{CO} region.

Initial form of catalyst	IR bands of carbonylated form of various platinum oxidation states, ν_{CO} (cm^{-1})								Refs
	$Pt^0(CO)$	$Pt^{\delta+}(CO)$	$Pt^+(CO)_2$	$Pt^+(CO)_3$	$Pt^{2+}(CO)$	$Pt^{2+}(CO)_2$	$Pt^{3+}(CO)$	$Pt^{3+}(CO)_2$	
1.1 ± 0.1 wt % Pt/SAPO-37					2123				this work
1.1 ± 0.1 wt % Pt/SAPO-37, after exposure to H_2 for 30 min		2092							this work
PtO_x/KLTL zeolite (oxidized)	_[a]	_[a]	_[a]	_[a]	2100	_[a]	_[a]	_[a]	11
3.0 wt% Pt/H-ZSM-5	_[a]	_[a]	2120, 2091	2162, 2150, 2110	2113	2165, 2150	2195	2211, 2175, or 2195	3
0.5 wt% Pt/H-mordenite	2123	_[a]	_[a]	_[a]	_[a]	_[a]	_[a]	_[a]	12
4.0 wt% Pt/NaY zeolite	_[a]	_[a]	_[a]	_[a]	2110	_[a]	_[a]	_[a]	13
0.2 wt% Pt/NaY zeolite	_[a]	2116	_[a]	_[a]	_[a]	_[a]	_[a]	_[a]	14
6 wt% Pt/NaY zeolite	_[a]	2100-2120	_[a]	_[a]	_[a]	_[a]	_[a]	_[a]	4
6 wt% Pt/NaX zeolite	2069	_[a]	2120, 2091	_[a]	2106	_[a]	2200	2216, 2188	4

[a]Not reported.

Table S3 shows the change of the isolated platinum species (initial species) supported on SAPO-37 under helium as they were exposed to ethylene, ethylene and H_2 (reaction conditions), ethylene at 353 K, and then helium.

Table S3. Summary of EXAFS fits parameters characterizing the structure of isolated platinum complexes supported on SAPO-37 at the Pt L_{III} edge as the feed composition is varied at room temperature and atmospheric pressure. *Denotes best fit model.

C_2H_4/H_2/He (molar ratio)	Model	Shell	N^a	10^3 x $\Delta\sigma^2$ ($Å^2$)[a]	R (Å)[a]	ΔE_0 (eV)[a]	Goodness of Fit	Notes
0:0:1	1*	O_s	4.0	5.9	2.02	-8.0	1.9876	Fig. S11 to S13; k range was from 5.0 to 13.0 Å; Error = 0.00063.
		O	2.0	2.4	2.29	-1.0		
		Al	1.0	1.8	2.70	-8.0		
		O_l	2.5	5.0	2.99	2.8		
	2	O_s	4	9.1	2.02	-8.0	2.4893	
		O	3	2.1	2.30	-4.0		
		Al	1.1	1.9	2.70	-10.0		
		O_l	2.4	4.8	3.00	1.0		
	3	O_s	4.0	2.6	2.02	-8.0	2.0500	
		O	2.1	5.3	2.30	-3.5		
		P	1.0	2.6	2.67	2.8		
		O_l	2.5	5.5	3.00	1.0		
1:10:1.5	1*	C	1.1	4.0	1.97	3.0	2.3616	Fig. S14; k range was from 3.0 to 10.0 Å; Error = 0.00174.
		O	1.6	5.0	2.12	-5.0		
		Pt	1.8	7.6	2.70	1.0		
1:10:1.5	1*	C	0.4	4.0	2.20	-1.8	1.3635	Fig. S15 to S17; k range was from 3.5 to 11.0 Å; Error = 0.00094.
		Pt	2.7	8.1	2.74	-2.5		
		O_l	1.5	4.0	2.97	-8.0		
	2	O	0.3	5.2	2.17	-8.0	1.5241	
		Pt	2.7	8.1	2.74	-4.0		
		O_l	1.5	3.7	2.97	-10.0		
	3	C	0.5	4.4	2.22	-4.6	1.4440	
		Pt	3.0	9.4	2.74	-3.5		
		C_l	1.1	3.8	2.78	-2.0		
		O_l	1.7	4.0	2.98	1.9		
1:0:1.5	1*	C	1.0	4.5	2.21	-8.0	2.1113	Fig. S18 to S20; k range was from 4.0 to 10.8 Å; Error = 0.00089.
		Pt	1.6	3.4	2.64	8.0		
		O_l	2.0	4.0	3.0	6.0		
		C_l	1.6	3.1	3.4	0.5		
	2	C	1.2	5.0	2.21	-8.0	2.8148	
		Pt	1.4	3.4	2.64	8.0		
		O_l	2.0	4.2	3.00	5.0		
		O_l	1.0	3.2	3.39	1.5		
	3	C	1.0	4.7	2.20	-6.0	2.5405	
		Pt	2.0	5.4	2.62	8.0		
		C_l	2.0	4.2	2.99	7.5		
		O_l	1.0	4.7	3.40	2.0		
0:0:1	1*	C	0.9	5.0	2.19	-8.0	0.88204	Fig. S21; k range was from 4.0 to 11.0 Å; Error = 0.00131.
		Pt	1.9	6.0	2.61	8.0		
		O_s	2.9	4.8	2.98	7.0		
		O_l	1.2	4.0	3.31	6.0		

[a]Notation: *N*, coordination number; *R*, distance between absorber and backscatter atoms; $\Delta\sigma^2$, Debye-Waller/disorder term; ΔE_0, inner potential. Subscripts: S, refers to an atom identified to be belonging to a short distance L, refers to the long contribution of an atom in the support.

Table S4. EXAFS models representing the data at the Pt L_{III} edge characterizing 1.1 ± 0.1 wt% platinum supported on SAPO-37 after exposure to flowing H_2 for 30 min at 298 K. The range in *k* was from 3.5 to 10.5 Å; error = 0.00075. *Denotes best fit model.

C_2H_4/H_2/He (molar ratio)	Model	Shell	*N*[a]	10^3 x $\Delta\sigma^2$ (Å^2)[a]	*R* (Å)[a]	ΔE_0 (eV)[a]	Goodness of Fit	Notes
0:0:1	1	O_s	1.0	9.0	2.02	-7.0	2.3760	Fig. S22 to S24.
		Pt	4.9	14.3	2.71	-8.0		
		O_l	1.0	4.7	3.44	-5.5		
		Al	1.1	9.3	3.94	-1.0		
	2*	O_s	1.0	11.8	2.03	-8.0	3.8995	
		Pt	4.0	3.8	2.71	-8.0		
		O_l	1.0	6.8	3.43	-1.7		
		Al	1.1	4.8	3.97	-4.0		
	3	O_s	1.0	9.0	2.03	-9.0	5.8575	
		Pt	3.9	12.7	2.71	-8.0		

[a]Notation: *N*, coordination number; *R*, distance between absorber and backscatter atoms; $\Delta\sigma^2$, Debye-Waller/disorder term; ΔE_0, inner potential. Subscripts: s, refers to an atom identified as belonging to the support; l, refers to the long Pt-scatterer contribution involving an atom in the support.

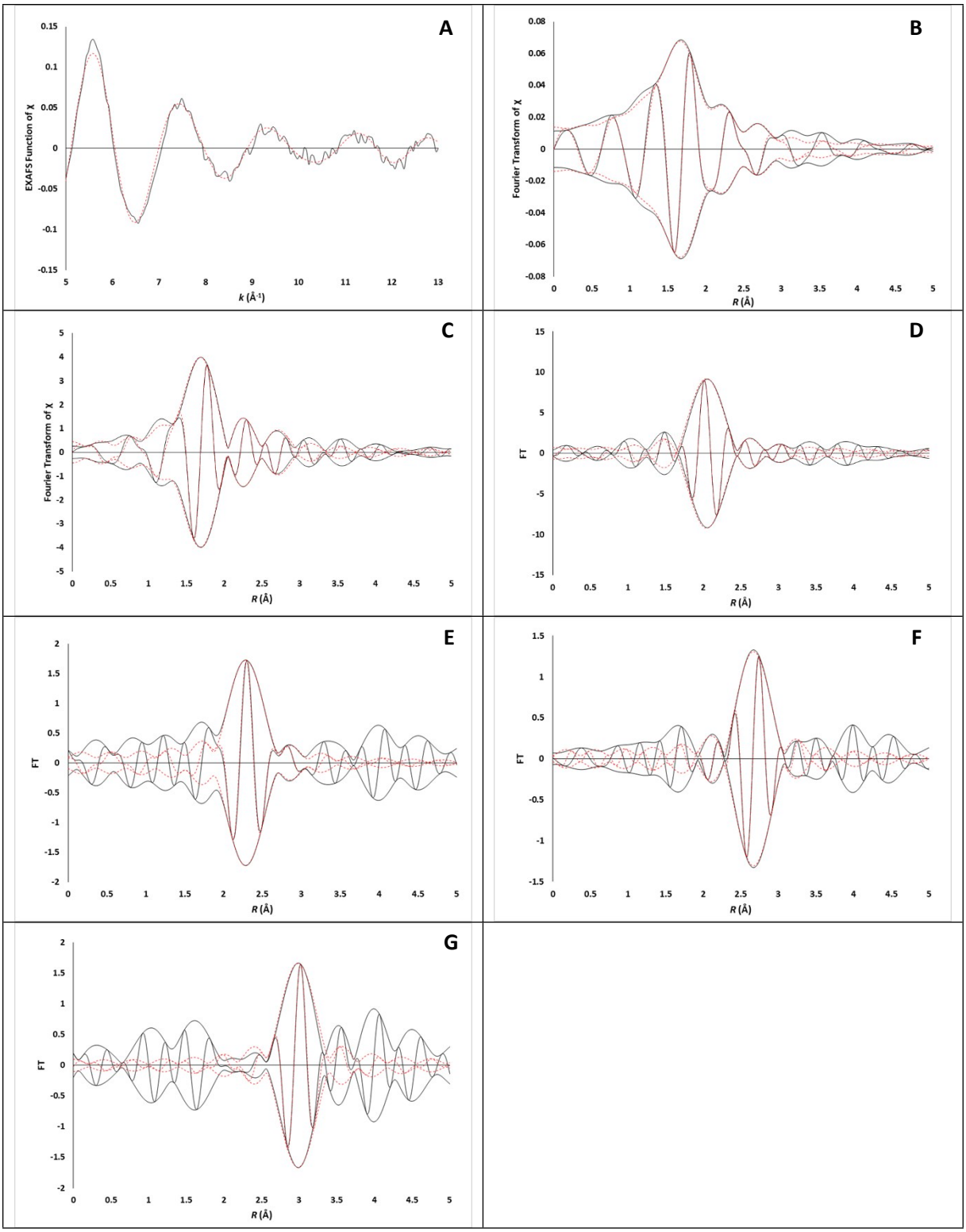

Fig. S11. EXAFS data recorded at Pt L_{III} edge characterizing the supported sample prepared from adsorption of $Pt(acac)_2$ on SAPO-37 in flowing helium at 298 K and 1 bar: (A) k^1-Weighted EXAFS function, $k^1(\chi)$ (solid line), and sum of the calculated contributions (dotted line). (B) k^1-Weighted imaginary part and magnitude of the Fourier transform of data (solid line) and sum of the calculated contributions (dotted line). (C) k^3-Weighted imaginary part and magnitude of the Fourier transform of data (solid line)

and sum of the calculated contributions (dotted line). (D) k^2-Weighted, phase- and amplitude-corrected, imaginary part and magnitude of the Fourier transform of data (solid line) and calculated contributions (dotted line) of Pt–O_{sup} shell. (E) k^2-Weighted, phase- and amplitude-corrected, imaginary part and magnitude of the Fourier transform of data (solid line) and calculated contributions (dotted line) of Pt–O shell. (F) k^2-Weighted, phase- and amplitude-corrected, imaginary part and magnitude of the Fourier transform of data (solid line) and calculated contributions (dotted line) of Pt–Al shell; (G) k^2-Weighted, phase- and amplitude-corrected, imaginary part and magnitude of the Fourier transform of data (solid line) and calculated contributions (dotted line) of Pt–O_l shell.

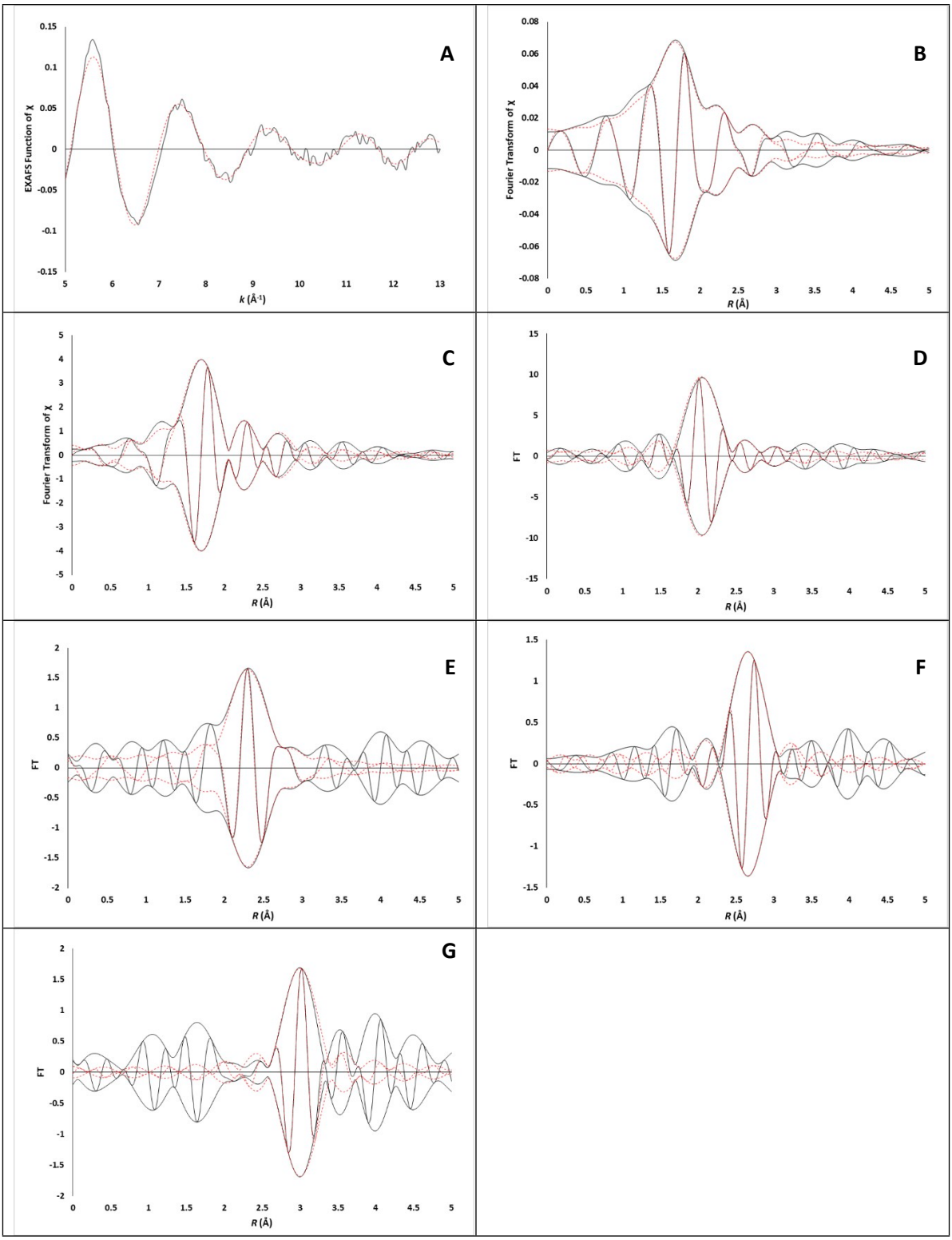

Fig. S12. EXAFS data recorded at Pt L_{III} edge characterizing the supported sample prepared from adsorption of $Pt(acac)_2$ on SAPO-37 in flowing helium at 298 K and 1 bar: (A) k^1-Weighted EXAFS function, $k^1(\chi)$ (solid line), and sum of the calculated contributions (dotted line). (B) k^1-Weighted imaginary part and magnitude of the Fourier transform of data (solid line) and sum of the calculated contributions (dotted line). (C) k^3-Weighted imaginary part and magnitude of the Fourier transform of data (solid line)

and sum of the calculated contributions (dotted line). (D) k^2-Weighted, phase- and amplitude-corrected, imaginary part and magnitude of the Fourier transform of data (solid line) and calculated contributions (dotted line) of Pt–O_{sup} shell. (E) k^2-Weighted, phase- and amplitude-corrected, imaginary part and magnitude of the Fourier transform of data (solid line) and calculated contributions (dotted line) of Pt–O shell. (F) k^2-Weighted, phase- and amplitude-corrected, imaginary part and magnitude of the Fourier transform of data (solid line) and calculated contributions (dotted line) of Pt–Al shell; (G) k^2-Weighted, phase- and amplitude-corrected, imaginary part and magnitude of the Fourier transform of data (solid line) and calculated contributions (dotted line) of Pt–O_l shell.

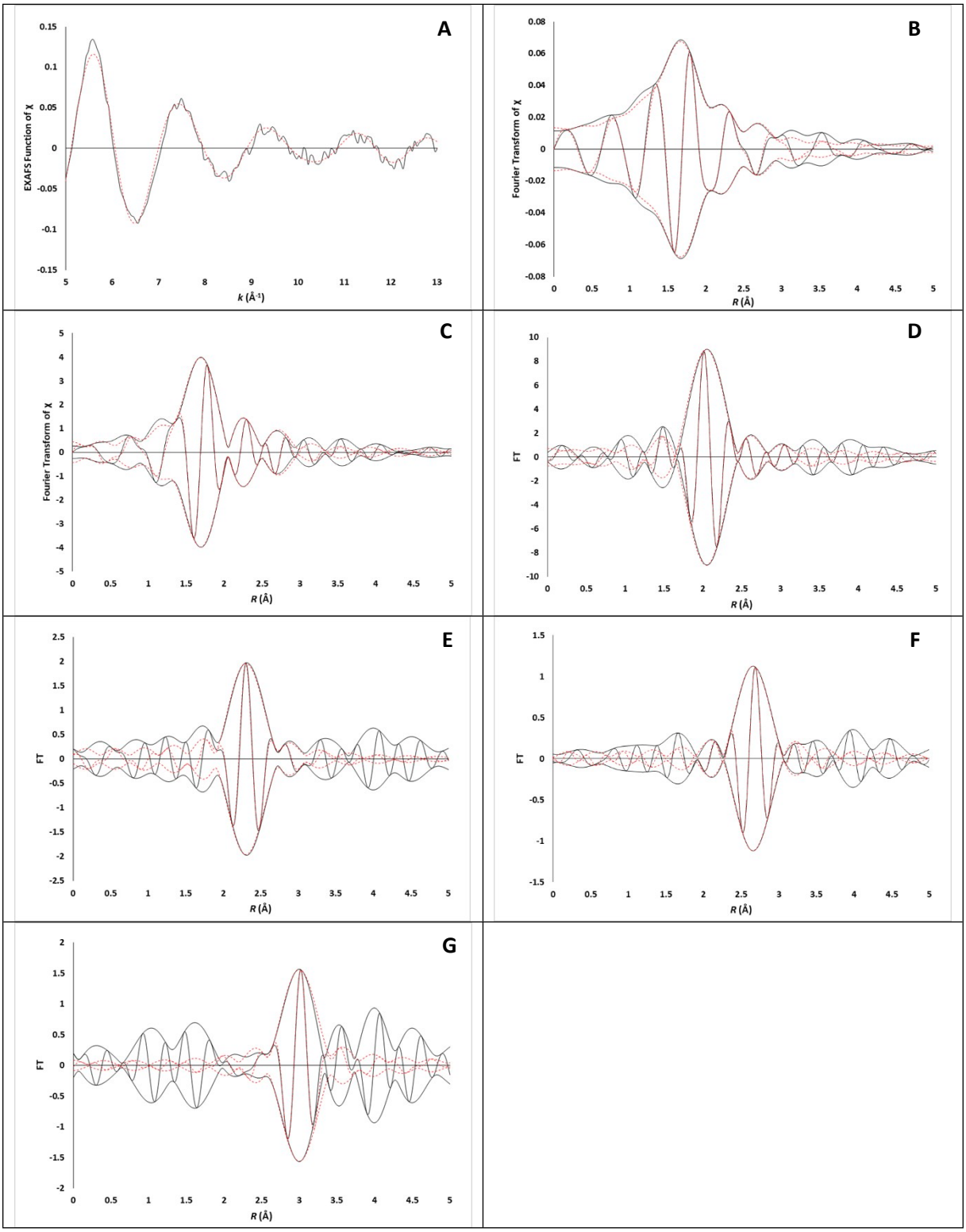

Fig. S13. EXAFS data recorded at Pt L_{III} edge characterizing the supported sample prepared from adsorption of $Pt(acac)_2$ on SAPO-37 in flowing helium at 298 K and 1 bar: (A) k^1-Weighted EXAFS function, $k^1(\chi)$ (solid line), and sum of the calculated contributions (dotted line). (B) k^1-Weighted imaginary part and magnitude of the Fourier transform of data (solid line) and sum of the calculated contributions

(dotted line). (C) k^3-Weighted imaginary part and magnitude of the Fourier transform of data (solid line) and sum of the calculated contributions (dotted line). (D) k^2-Weighted, phase- and amplitude-corrected, imaginary part and magnitude of the Fourier transform of data (solid line) and calculated contributions (dotted line) of Pt–O_{sup} shell. (E) k^2-Weighted, phase- and amplitude-corrected, imaginary part and magnitude of the Fourier transform of data (solid line) and calculated contributions (dotted line) of Pt–O shell; (F) k^2-Weighted, phase- and amplitude-corrected, imaginary part and magnitude of the Fourier transform of data (solid line) and calculated contributions (dotted line) of Pt–P shell. (G) k^2-Weighted, phase- and amplitude-corrected, imaginary part and magnitude of the Fourier transform of data (solid line) and calculated contributions (dotted line) of Pt–O_l shell.

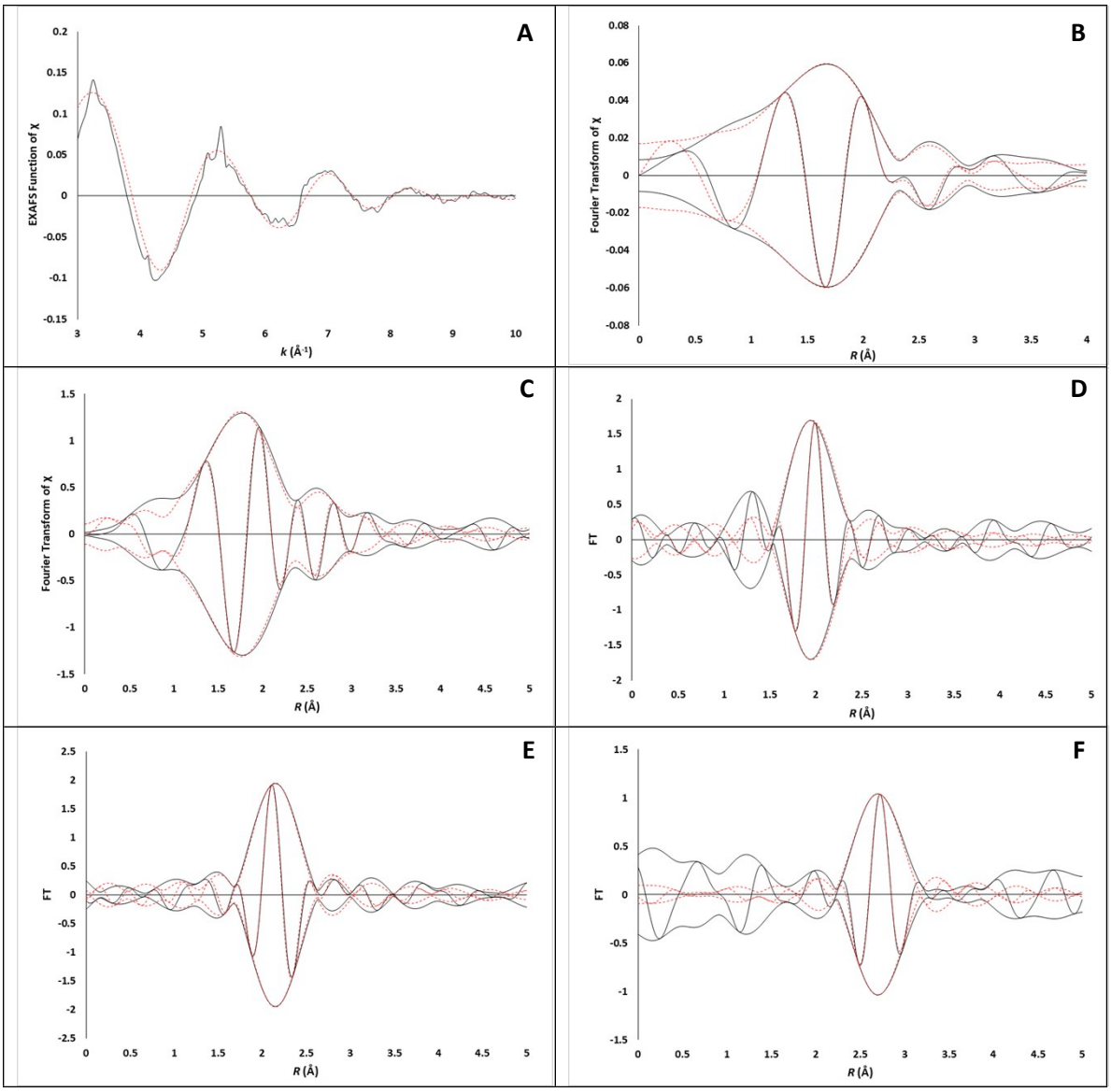

Fig. S14. EXAFS data recorded at Pt L_{III} edge characterizing the supported sample prepared from adsorption of $Pt(acac)_2$ on SAPO-37 in flowing ethylene and hydrogen at 298 K and 1 bar: (A) k^1-Weighted EXAFS function, $k^1(\chi)$ (solid line), and sum of the calculated contributions (dotted line). (B) k^1-Weighted imaginary part and magnitude of the Fourier transform of data (solid line) and sum of the calculated contributions (dotted line). (C) k^3-Weighted imaginary part and magnitude of the Fourier transform of data (solid line) and sum of the calculated contributions (dotted line). (D) k^2-Weighted, phase- and amplitude-corrected, imaginary part and magnitude of the Fourier transform of data (solid line) and calculated contributions (dotted line) of Pt–C shell. (E) k^2-Weighted, phase- and amplitude-corrected, imaginary part and magnitude of the Fourier transform of data (solid line) and calculated contributions (dotted line) of Pt–O shell. (F) k^2-Weighted, phase- and amplitude-corrected, imaginary part and magnitude of the Fourier transform of data (solid line) and calculated contributions (dotted line) of Pt–Pt shell.

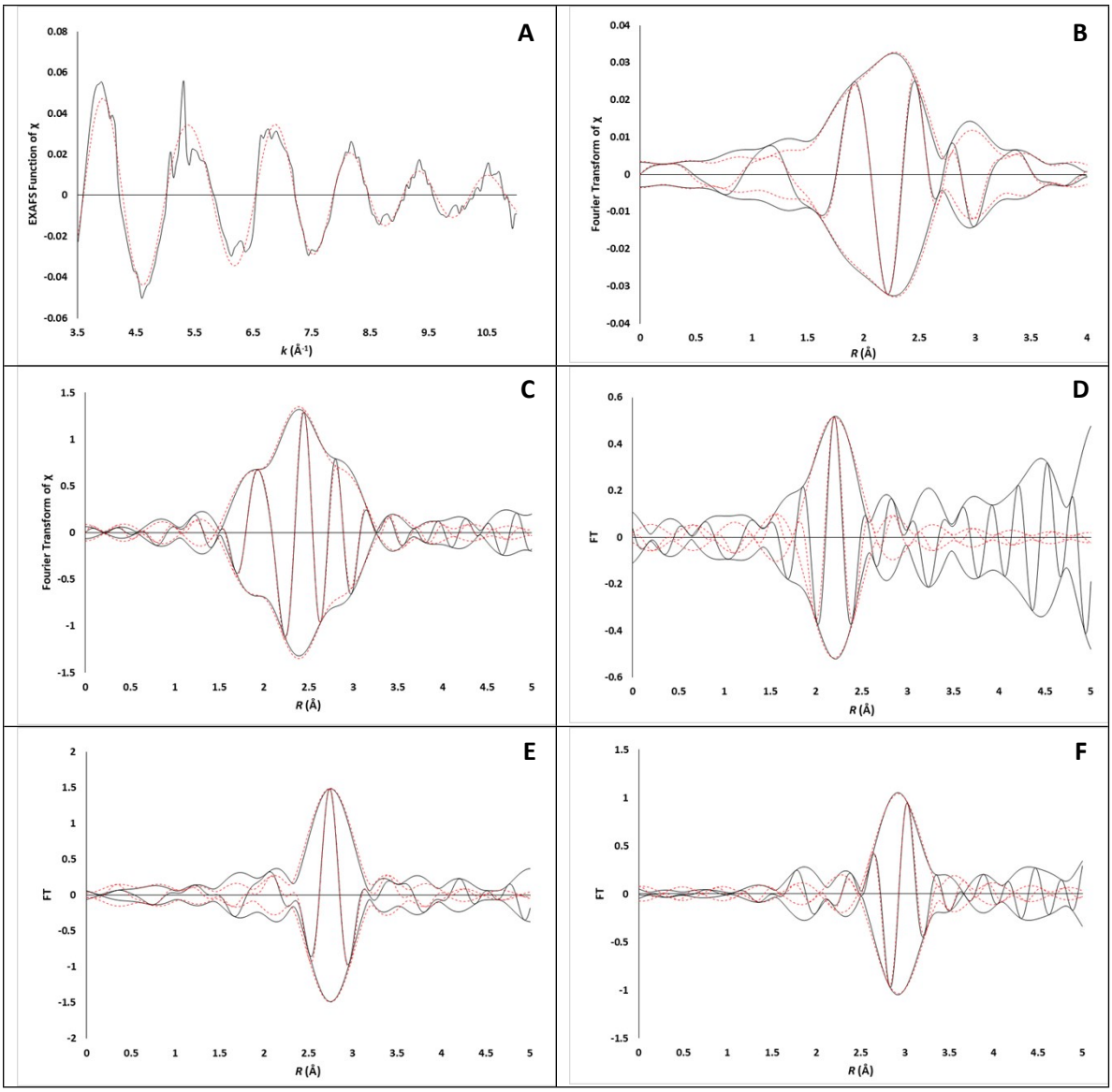

Fig. S15. EXAFS data recorded at Pt L_{III} edge characterizing the supported sample prepared from adsorption of $Pt(acac)_2$ on SAPO-37 in flowing ethylene and hydrogen at 298 K and 1 bar: (A) k^1-Weighted EXAFS function, $k^1(\chi)$ (solid line), and sum of the calculated contributions (dotted line). (B) k^1-Weighted imaginary part and magnitude of the Fourier transform of data (solid line) and sum of the calculated contributions (dotted line). (C) k^3-Weighted imaginary part and magnitude of the Fourier transform of data (solid line) and sum of the calculated contributions (dotted line). (D) k^2-Weighted, phase- and amplitude-corrected, imaginary part and magnitude of the Fourier transform of data (solid line) and calculated contributions (dotted line) of Pt–C shell. (E) k^2-Weighted, phase- and amplitude-corrected, imaginary part and magnitude of the Fourier transform of data (solid line) and calculated contributions (dotted line) of Pt–Pt shell. (F) k^2-Weighted, phase- and amplitude-corrected, imaginary part and magnitude of the Fourier transform of data (solid line) and calculated contributions (dotted line) of Pt–O_1 shell.

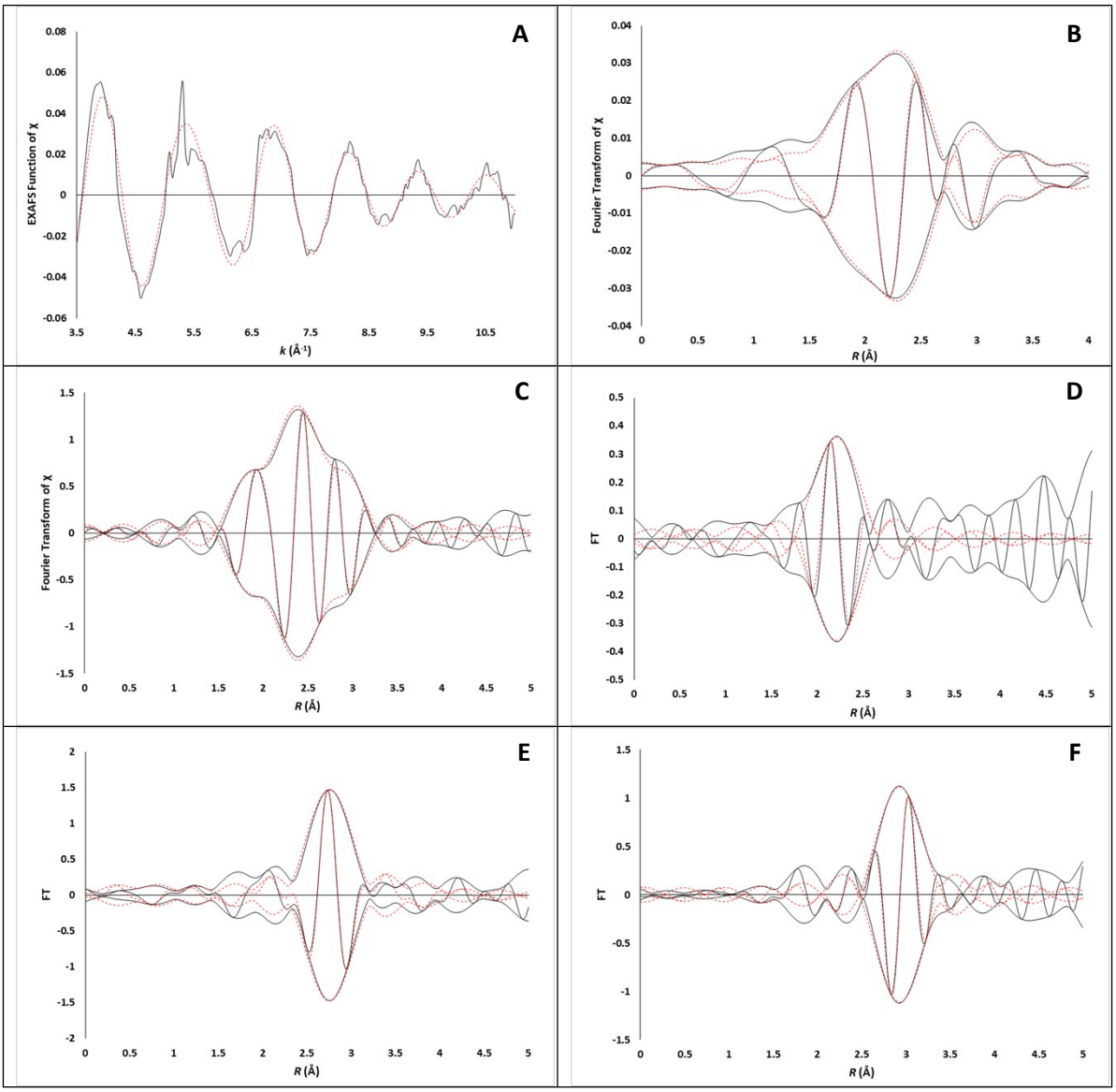

Fig. S16. EXAFS data recorded at Pt L_{III} edge characterizing the supported sample prepared from adsorption of $Pt(acac)_2$ on SAPO-37 in flowing ethylene and hydrogen at 298 K and 1 bar: (A) k^1-Weighted EXAFS function, $k^1(\chi)$ (solid line), and sum of the calculated contributions (dotted line). (B) k^1-Weighted imaginary part and magnitude of the Fourier transform of data (solid line) and sum of the calculated contributions (dotted line). (C) k^3-Weighted imaginary part and magnitude of the Fourier transform of data (solid line) and sum of the calculated contributions (dotted line). (D) k^2-Weighted, phase- and amplitude-corrected, imaginary part and magnitude of the Fourier transform of data (solid line) and calculated contributions (dotted line) of Pt–O shell; (E) k^2-Weighted, phase- and amplitude-corrected, imaginary part and magnitude of the Fourier transform of data (solid line) and calculated contributions (dotted line) of Pt–Pt shell; (F) k^2-Weighted, phase- and amplitude-corrected, imaginary part and magnitude of the Fourier transform of data (solid line) and calculated contributions (dotted line) of Pt–O_l shell.

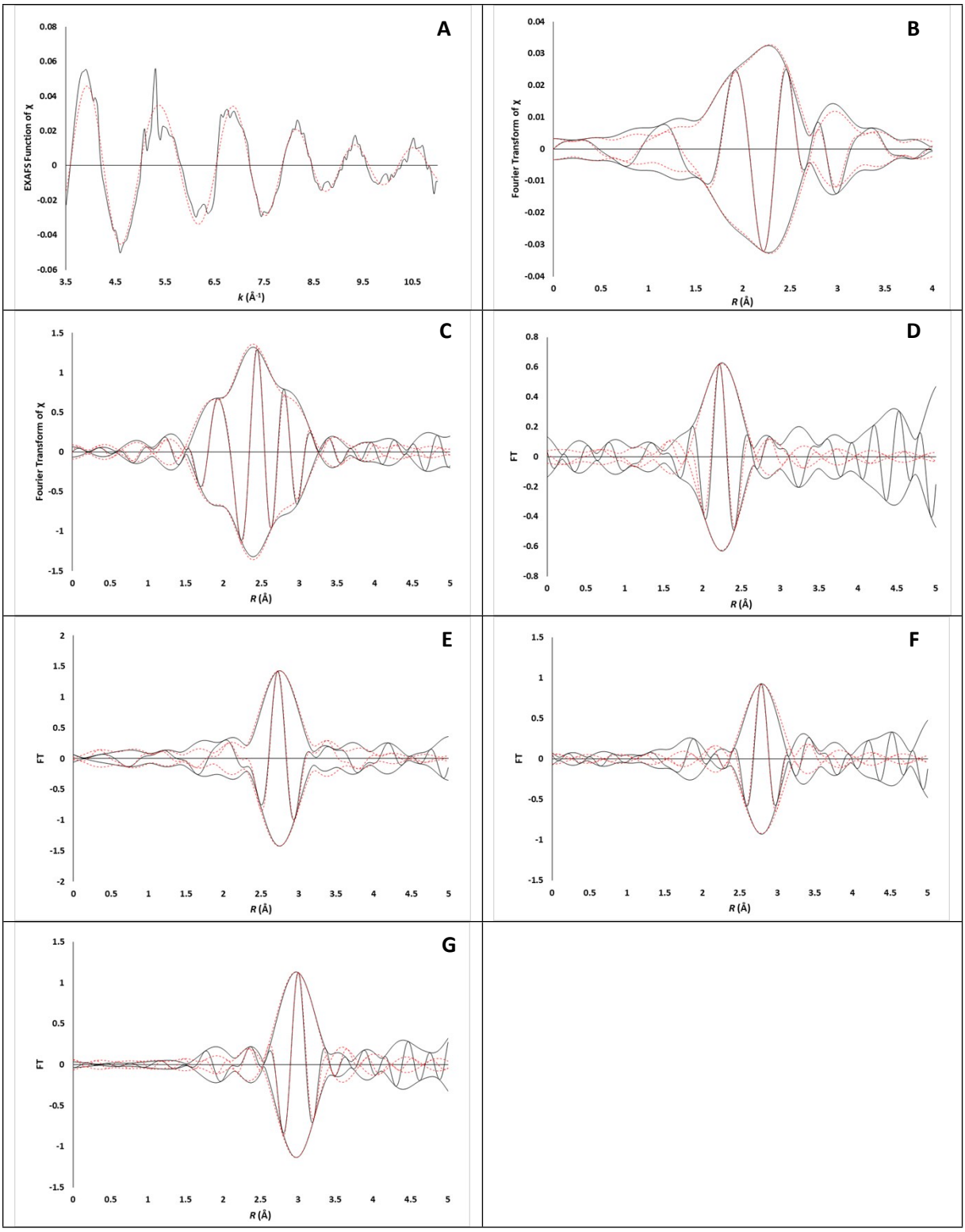

Fig. S17. EXAFS data recorded at Pt L_{III} edge characterizing the supported sample prepared from adsorption of $Pt(acac)_2$ on SAPO-37 in flowing ethylene and hydrogen at 298 K and 1 bar: (A) k^1-Weighted EXAFS function, $k^1(\chi)$ (solid line), and sum of the calculated contributions (dotted line). (B) k^1-Weighted imaginary part and magnitude of the Fourier transform of data (solid line) and sum of the calculated contributions (dotted line). (C) k^3-Weighted imaginary part and magnitude of the Fourier transform of data

(solid line) and sum of the calculated contributions (dotted line). (D) k^2-Weighted, phase- and amplitude-corrected, imaginary part and magnitude of the Fourier transform of data (solid line) and calculated contributions (dotted line) of Pt–C shell; (E) k^2-Weighted, phase- and amplitude-corrected, imaginary part and magnitude of the Fourier transform of data (solid line) and calculated contributions (dotted line) of Pt–Pt shell; (F) k^2-Weighted, phase- and amplitude-corrected, imaginary part and magnitude of the Fourier transform of data (solid line) and calculated contributions (dotted line) of Pt–C_l shell; (G) k^2-Weighted, phase- and amplitude-corrected, imaginary part and magnitude of the Fourier transform of data (solid line) and calculated contributions (dotted line) of Pt–O_l shell.

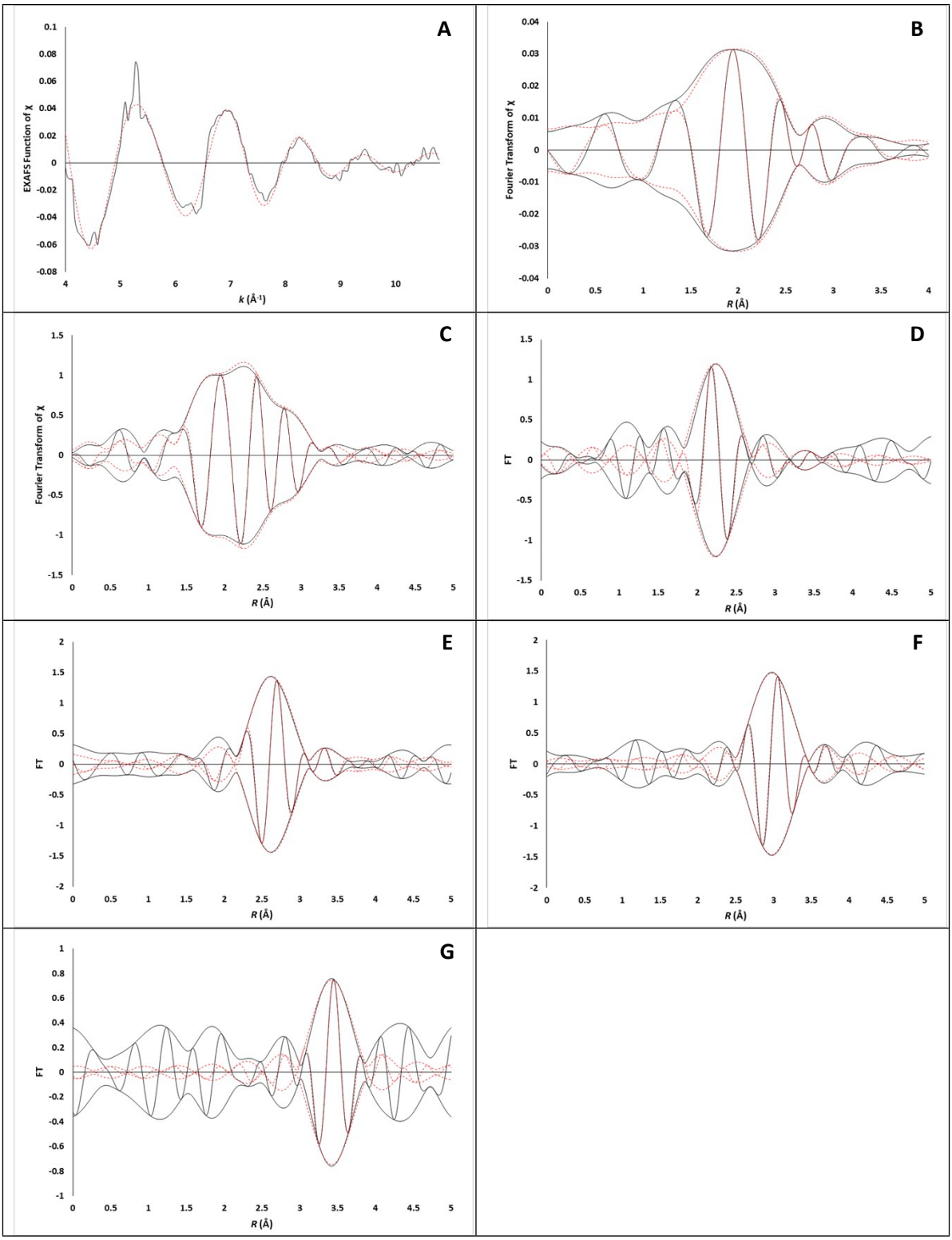

Fig. S18. EXAFS data recorded at Pt L_{III} edge characterizing the supported sample prepared from adsorption of $Pt(acac)_2$ on SAPO-37 in flowing ethylene after reaction conditions at 298 K and 1 bar: (A) k^1-Weighted EXAFS function, $k^1(\chi)$ (solid line), and sum of the calculated contributions (dotted line). (B) k^1-Weighted imaginary part and magnitude of the Fourier transform of data (solid line) and sum of the calculated contributions (dotted line). (C) k^3-Weighted imaginary part and magnitude of the Fourier

transform of data (solid line) and sum of the calculated contributions (dotted line). (D) k^2-Weighted, phase- and amplitude-corrected, imaginary part and magnitude of the Fourier transform of data (solid line) and calculated contributions (dotted line) of Pt–C shell. (E) k^2-Weighted, phase- and amplitude-corrected, imaginary part and magnitude of the Fourier transform of data (solid line) and calculated contributions (dotted line) of Pt–Pt shell. (F) k^2-Weighted, phase- and amplitude-corrected, imaginary part and magnitude of the Fourier transform of data (solid line) and calculated contributions (dotted line) of Pt–O shell. (G) k^2-Weighted, phase- and amplitude-corrected, imaginary part and magnitude of the Fourier transform of data (solid line) and calculated contributions (dotted line) of Pt–C_1 shell.

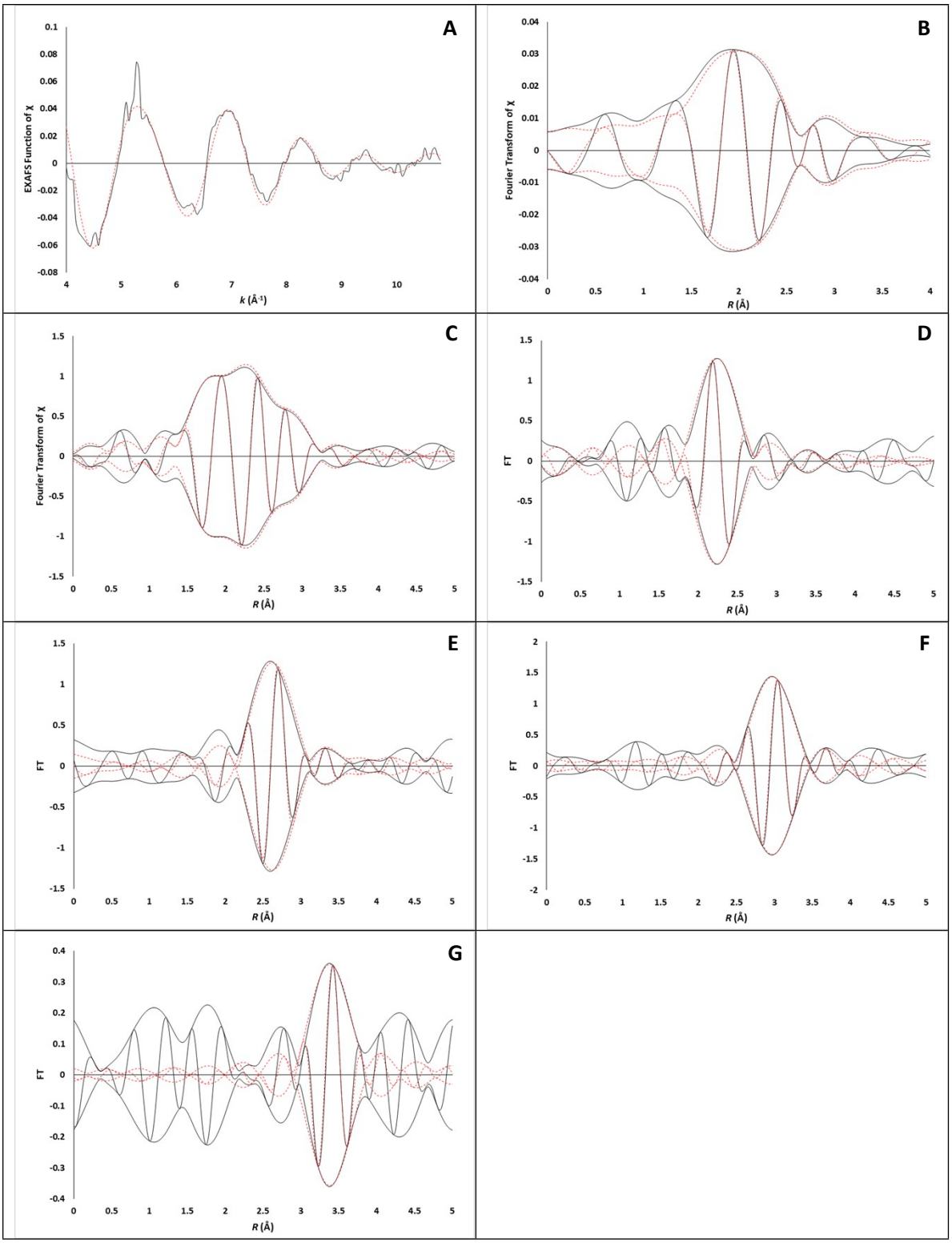

Fig. S19. EXAFS data recorded at Pt L_{III} edge characterizing the supported sample prepared from adsorption of $Pt(acac)_2$ on SAPO-37 in flowing ethylene after reaction conditions at 298 K and 1 bar: (A) k^1-Weighted EXAFS function, $k^1(\chi)$ (solid line), and sum of the calculated contributions (dotted line). (B) k^1-Weighted imaginary part and magnitude of the Fourier transform of data (solid line) and sum of the calculated contributions (dotted line). (C) k^3-Weighted imaginary part and magnitude of the Fourier

transform of data (solid line) and sum of the calculated contributions (dotted line). (D) k^2-Weighted, phase- and amplitude-corrected, imaginary part and magnitude of the Fourier transform of data (solid line) and calculated contributions (dotted line) of Pt–C shell; (E) k^2-Weighted, phase- and amplitude-corrected, imaginary part and magnitude of the Fourier transform of data (solid line) and calculated contributions (dotted line) of Pt–Pt shell; (F) k^2-Weighted, phase- and amplitude-corrected, imaginary part and magnitude of the Fourier transform of data (solid line) and calculated contributions (dotted line) of Pt–O shell (G) k^2-Weighted, phase- and amplitude-corrected, imaginary part and magnitude of the Fourier transform of data (solid line) and calculated contributions (dotted line) of Pt–O_l shell.

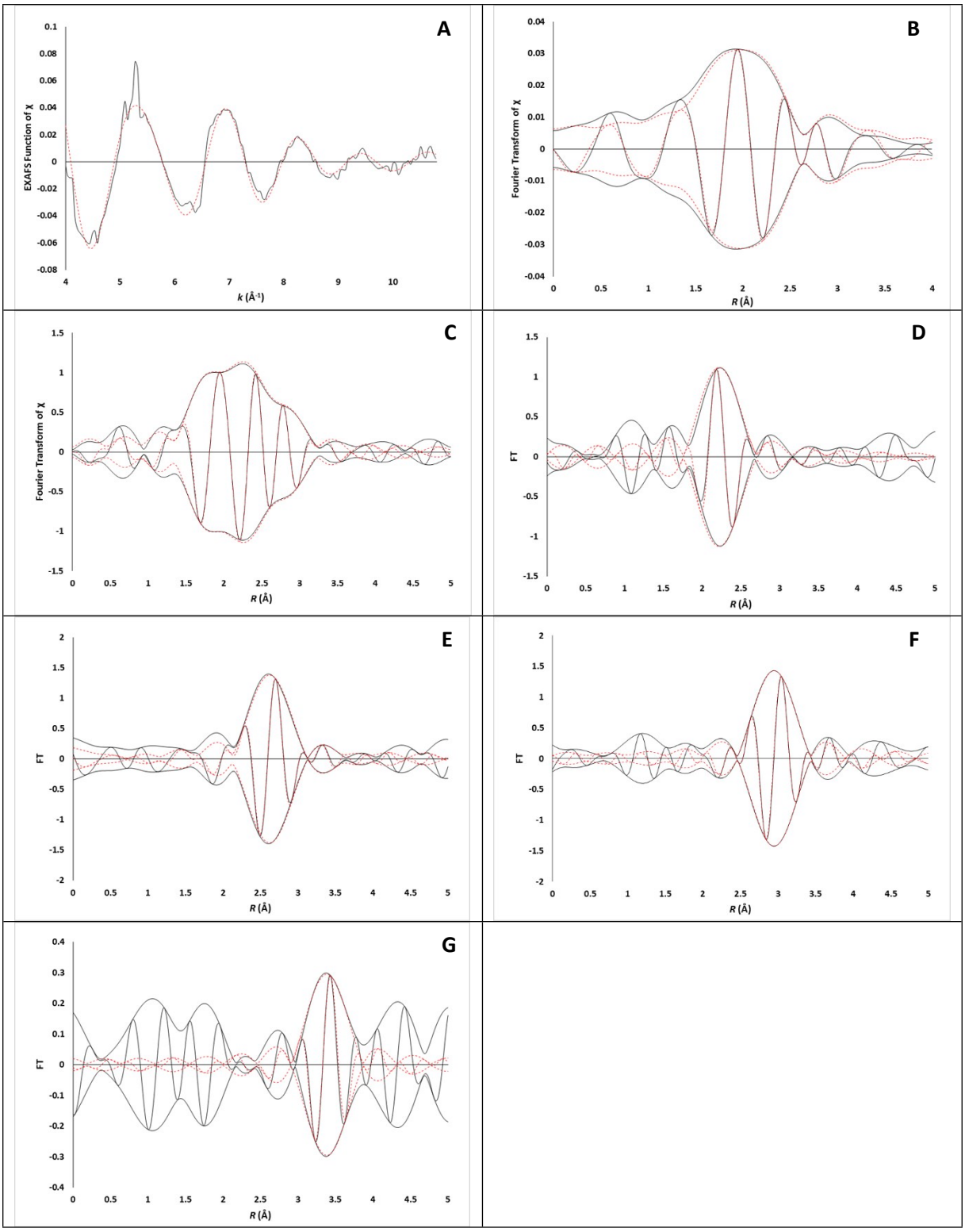

Fig. S20. EXAFS data recorded at Pt L_{III} edge characterizing the supported sample prepared from adsorption of $Pt(acac)_2$ on SAPO-37 in flowing ethylene after reaction conditions at 298 K and 1 bar: (A) k^1-Weighted EXAFS function, $k^1(\chi)$ (solid line), and sum of the calculated contributions (dotted line). (B) k^1-Weighted imaginary part and magnitude of the Fourier transform of data (solid line) and sum of the calculated contributions (dotted line). (C) k^3-Weighted imaginary part and magnitude of the Fourier

transform of data (solid line) and sum of the calculated contributions (dotted line). (D) k^2-Weighted, phase- and amplitude-corrected, imaginary part and magnitude of the Fourier transform of data (solid line) and calculated contributions (dotted line) of Pt–C shell; (E) k^2-Weighted, phase- and amplitude-corrected, imaginary part and magnitude of the Fourier transform of data (solid line) and calculated contributions (dotted line) of Pt–Pt shell; (F) k^2-Weighted, phase- and amplitude-corrected, imaginary part and magnitude of the Fourier transform of data (solid line) and calculated contributions (dotted line) of Pt–O shell (G) k^2-Weighted, phase- and amplitude-corrected, imaginary part and magnitude of the Fourier transform of data (solid line) and calculated contributions (dotted line) of Pt–O_l shell.

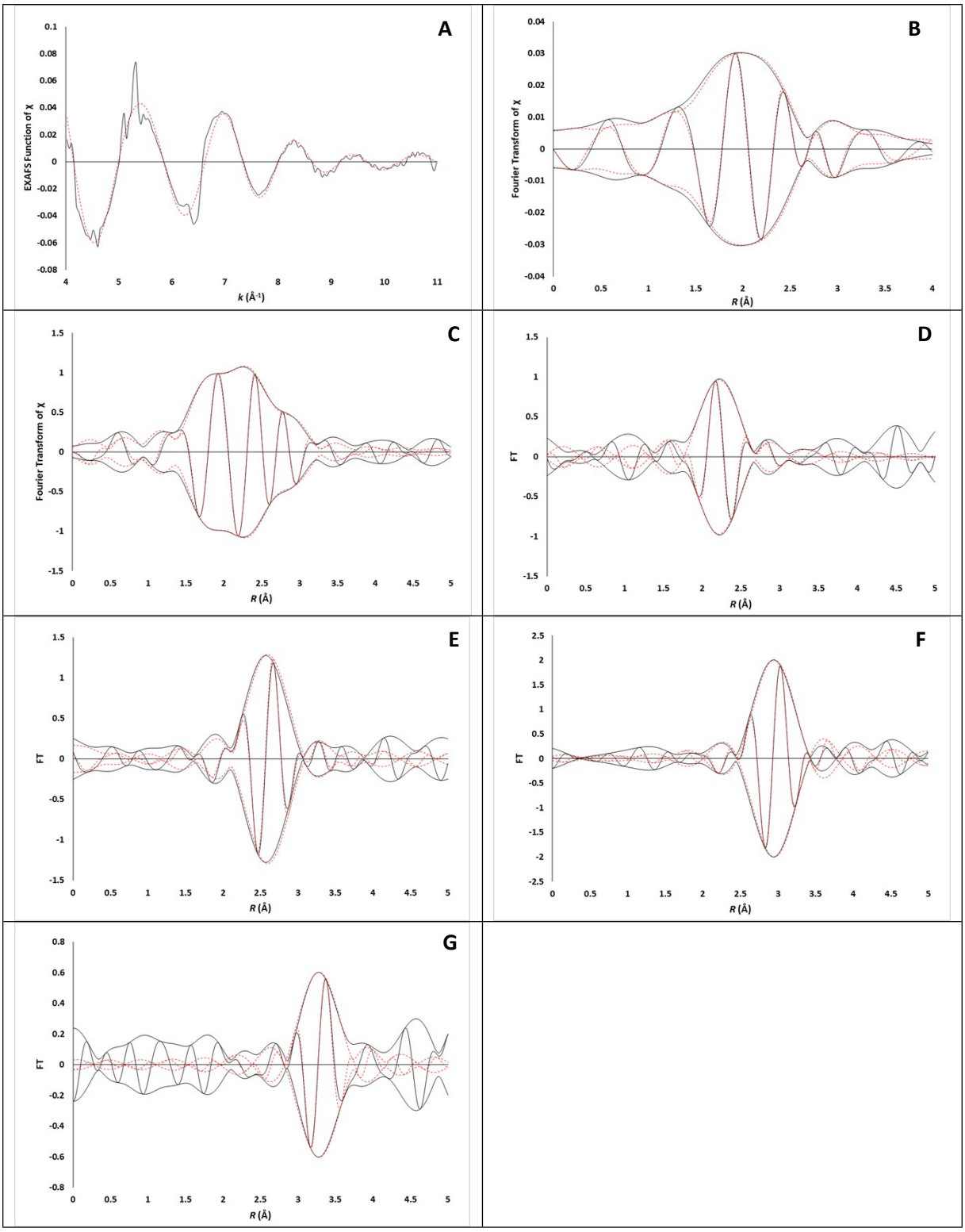

Fig. S21. EXAFS data recorded at Pt L_{III} edge characterizing the supported sample prepared from adsorption of $Pt(acac)_2$ on SAPO-37 in flowing helium at 298 K and 1 bar after exposure to reaction conditions and an ethylene treatment at 353 K: (A) k^1-Weighted EXAFS function, $k^1(\chi)$ (solid line), and sum of the calculated contributions (dotted line). (B) k^1-Weighted imaginary part and magnitude of the Fourier transform of data (solid line) and sum of the calculated contributions (dotted line). (C) k^3-Weighted

imaginary part and magnitude of the Fourier transform of data (solid line) and sum of the calculated contributions (dotted line). (D) k^2-Weighted, phase- and amplitude-corrected, imaginary part and magnitude of the Fourier transform of data (solid line) and calculated contributions (dotted line) of Pt–C shell; (E) k^2-Weighted, phase- and amplitude-corrected, imaginary part and magnitude of the Fourier transform of data (solid line) and calculated contributions (dotted line) of Pt–Pt shell; (F) k^2-Weighted, phase- and amplitude-corrected, imaginary part and magnitude of the Fourier transform of data (solid line) and calculated contributions (dotted line) of Pt–O_s shell; (G) k^2-Weighted, phase- and amplitude-corrected, imaginary part and magnitude of the Fourier transform of data (solid line) and calculated contributions (dotted line) of Pt–O_l shell.

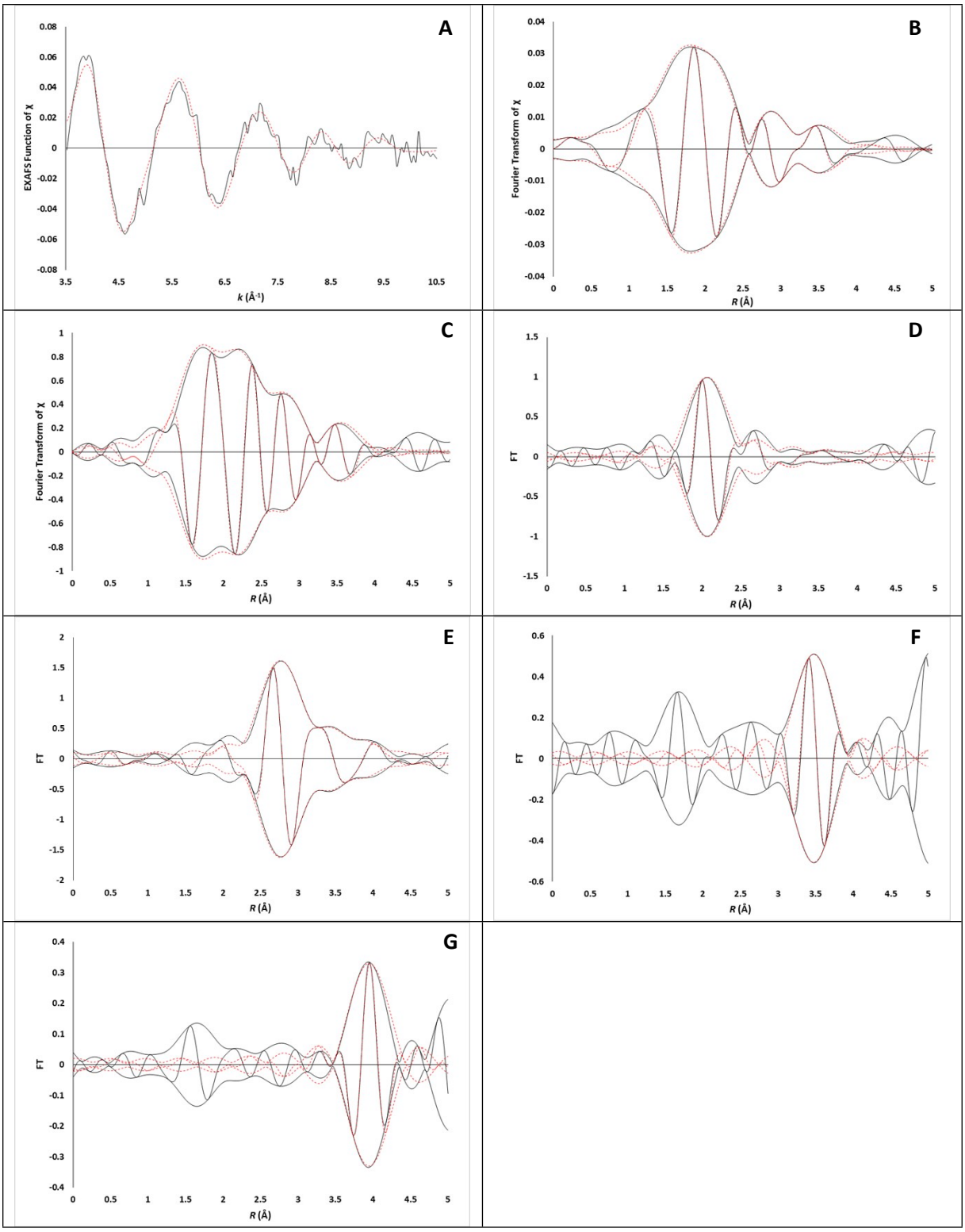

Fig. S22. EXAFS data recorded at Pt L_{III} edge characterizing the supported sample prepared from adsorption of $Pt(acac)_2$ on SAPO-37 in flowing helium at 298 K and 1 bar after exposure to hydrogen for 1 h: (A) k^1-Weighted EXAFS function, $k^1(\chi)$ (solid line), and sum of the calculated contributions (dotted line). (B) k^1-Weighted imaginary part and magnitude of the Fourier transform of data (solid line) and sum of the calculated contributions (dotted line). (C) k^3-Weighted imaginary part and magnitude of the Fourier

transform of data (solid line) and sum of the calculated contributions (dotted line). (D) k^2-Weighted, phase- and amplitude-corrected, imaginary part and magnitude of the Fourier transform of data (solid line) and calculated contributions (dotted line) of Pt–O_{sup} shell; (E) k^2-Weighted, phase- and amplitude-corrected, imaginary part and magnitude of the Fourier transform of data (solid line) and calculated contributions (dotted line) of Pt–Pt shell; (F) k^2-Weighted, phase- and amplitude-corrected, imaginary part and magnitude of the Fourier transform of data (solid line) and calculated contributions (dotted line) of Pt–O_l shell; (G) k^2-Weighted, phase- and amplitude-corrected, imaginary part and magnitude of the Fourier transform of data (solid line) and calculated contributions (dotted line) of Pt–Al shell.

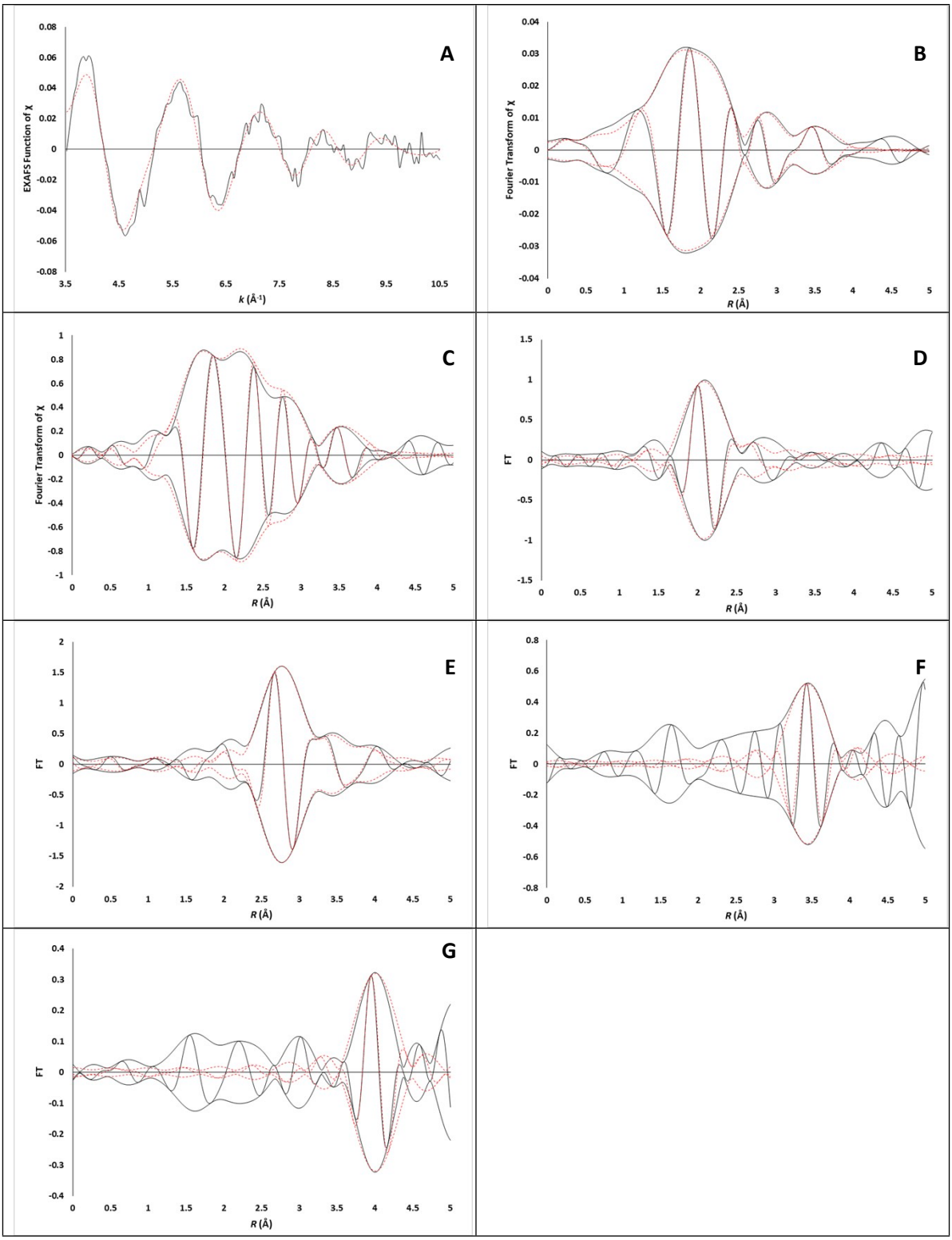

Fig. S23. EXAFS data recorded at Pt L_{III} edge characterizing the supported sample prepared from adsorption of $Pt(acac)_2$ on SAPO-37 in flowing helium at 298 K and 1 bar after exposure to hydrogen for 1 h: (A) k^1-Weighted EXAFS function, $k^1(\chi)$ (solid line), and sum of the calculated contributions (dotted line). (B) k^1-Weighted imaginary part and magnitude of the Fourier transform of data (solid line) and sum of the calculated contributions (dotted line). (C) k^3-Weighted imaginary part and magnitude of the Fourier

transform of data (solid line) and sum of the calculated contributions (dotted line). (D) k^2-Weighted, phase- and amplitude-corrected, imaginary part and magnitude of the Fourier transform of data (solid line) and calculated contributions (dotted line) of Pt–O_{sup} shell; (E) k^2-Weighted, phase- and amplitude-corrected, imaginary part and magnitude of the Fourier transform of data (solid line) and calculated contributions (dotted line) of Pt–Pt shell; (F) k^2-Weighted, phase- and amplitude-corrected, imaginary part and magnitude of the Fourier transform of data (solid line) and calculated contributions (dotted line) of Pt– O_l shell; (G) k^2-Weighted, phase- and amplitude-corrected, imaginary part and magnitude of the Fourier transform of data (solid line) and calculated contributions (dotted line) of Pt–Al shell.

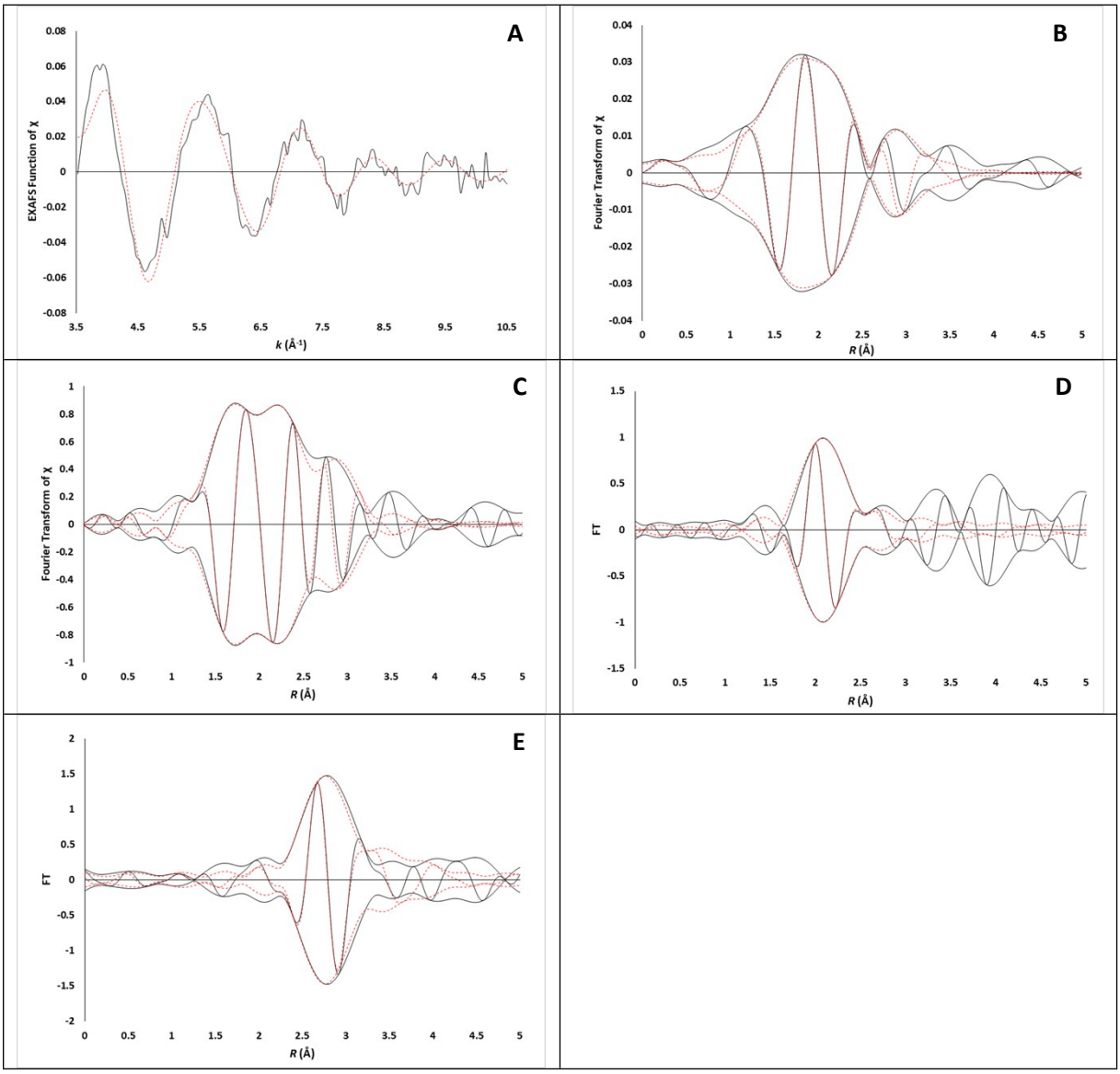

Fig. S24. EXAFS data recorded at Pt L_{III} edge characterizing the supported sample prepared from adsorption of $Pt(acac)_2$ on SAPO-37 in flowing helium at 298 K and 1 bar after exposure to hydrogen for 1 h: (A) k^1-Weighted EXAFS function, $k^1(\chi)$ (solid line), and sum of the calculated contributions (dotted line). (B) k^1-Weighted imaginary part and magnitude of the Fourier transform of data (solid line) and sum of the calculated contributions (dotted line). (C) k^3-Weighted imaginary part and magnitude of the Fourier transform of data (solid line) and sum of the calculated contributions (dotted line). (D) k^2-Weighted, phase- and amplitude-corrected, imaginary part and magnitude of the Fourier transform of data (solid line) and calculated contributions (dotted line) of Pt–O_{sup} shell; (E) k^2-Weighted, phase- and amplitude-corrected, imaginary part and magnitude of the Fourier transform of data (solid line) and calculated contributions (dotted line) of Pt–Pt shell.

References

1 K.I. Hadjiivanov, G.N. Vayssilov, Characterization of oxide surfaces and zeolites by carbon monoxide as an IR probe molecule, *Adv. Catal.*, 2002, **47**, 307–511.

2 K. Ding, A. Gulec, A.M. Johnson, N.M. Schweitzer, G.D. Stucky, L.D. Marks, P.C. Stair, Identification of active sites in CO oxidation and water-gas shift over supported Pt catalysts, *Science*, 2015, **350**, 189–192.

3 K. Chakarova, M. Mihaylov, K. Hadjiivanov, FTIR spectroscopic study of CO adsorption on Pt-H-ZSM-5, *Micropor. Mesopor.Mater.*, 2005, **81**, 305–312.

4 Y. Akdogan, C. Vogt, M. Bauer, H. Bertagnolli, L. Giurgiu, E. Roduner, Platinum species in the pores of NaX, NaY and NaA zeolites studied using EPR, XAS and FTIR spectroscopies, *Phys. Chem. Chem. Phys.*, 2008, **10**, 2952–2963.

5 H. Miessner, D. Gutschick, H. Ewald, H. Müller, The Influence of Support on the Geminal Dicarbonyl Species $Rh^{I}(CO)_2$ on Supported Rhodium Catalysts: an IR Spectroscopic Study, *J. Mol. Catal.*, 1986, **36**, 359–373.

6 J. Howard, P.J. Lux, J. Yarwood, A Fourier-transform i.r. study of ethene adsorbed on HZSM-5 zeolite at low temperature (295 K), *Zeolites*, 1988, **8**, 427–431.

7 J.E. Perez-Aguilar, C.Y. Chen, J.T. Hughes, C.Y. Fang, B.C. Gates, Isostructural Atomically Dispersed Rhodium Catalysts Supported on SAPO-37 and on HY Zeolite, *J. Am. Chem. Soc.*, 2020, **142**, 11474–11485.

8 J. Guzman, B.G. Anderson, C.P. Vinod, K. Ramesh, J.W. Niemantsverdriet, B.C. Gates, Synthesis and reactivity of dimethyl gold complexes supported on MgO: Characterization by infrared and X-ray absorption spectroscopies, *Langmuir*, 2005, **21**, 3675–3683.

9 M. Zhou, R.H. Crabtree, C–H oxidation by platinum group metal oxo or peroxo species, *Chem. Soc. Rev.*, 2011, **40**, 1875–1884.

10 M.S. Davies, T.W. Hambley, $[Pt_2Cl_2(\mu_2\text{-}O_2)_2([9]aneN_3)_2]Cl_2$: A Novel Platinum(IV) Dimer with

Two Bridging Peroxo Ligands that Provides Insight into the Mechanism of Aerial Oxidation of Platinum(II), *Inorg. Chem.*, 1998, **37**, 5408–5409.

11 J.D. Kistler, N. Chotigkrai, P. Xu, B. Enderle, P. Praserthdam, C.Y. Chen, N.D. Browning, B.C. Gates, A single-site platinum CO oxidation catalyst in zeolite KLTL: Microscopic and spectroscopic determination of the locations of the platinum atoms, *Angew. Chem. Int. Ed.*, 2014, **53**, 8904–8907.

12 V.L. Zholobenko, G.D. Lei, B.T. Carvill, B.A. Lerner, W.M.H. Sachtler, Identification of isolated Pt atoms in H-mordenite, *J. Chem. Soc. Faraday Trans.*, 1994, **90**, 233–238.

13 G. Li, T. Fujimoto, A. Fukuoka, EXAFS and Fourier transform IR Characterization of Platinum Carbonyl Clusters $[Pt_3(CO)_6]_n^{2-}$ (n = 3, 4) encapsulated in NaY zeolites and Their Effective Catalysis in the CO + NO Reaction, *J. Chem. Soc. Chem. Commun.*, 1991, **3**, 1337–1339.

14 Y. Liu, Z. Li, Q. Yu, Y. Chen, Z. Chai, G. Zhao, S. Liu, W.C. Cheong, Y. Pan, Q. Zhang, L. Gu, L. Zheng, Y. Wang, Y. Lu, D. Wang, C. Chen, Q. Peng, Y. Liu, L. Liu, J. Chen, Y. Li, A General Strategy for Fabricating Isolated Single Metal Atomic Site Catalysts in y Zeolite, *J. Am. Chem. Soc.*, 2019, **141**, 9305–9311.